Magnetic Resonance Imaging-Guided Needle Insertion Robots

A Review of Systems for Liver and Kidney Interventions

By Ziting Liang, Lukas Lindenroth, Ryman Hashem, Steve Bandula, Danail Stoyanov, and Agostino Stilli

Magnetic resonance imaging (MRI)-guided intervention for the liver and kidney has achieved considerable progress in tumor diagnosis and treatment over the past two decades. However, due to the space constraints associated with the narrow and deep bore of MRI machines, it is still extremely challenging for clinicians to position and drive the needle-shaped probes used for delivering the treatment where the targeted tumoral mass is located. MRI-compatible robotic systems have been investigated by several research teams worldwide, both in academia and industry. These endeavors aim to address challenges related to the confined workspace within MRI machine bores. The goal is to facilitate the shift from computed tomography (CT)-guided to MRI-guided interventions, leveraging the advantages of MRI, including its exceptional soft tissue contrast, nonionizing radiation, and versatile multiangle imaging capabilities. In this article, we systematically review the state-of-the-art MRI-guided needle insertion robots for the treatment of the liver and kidney in order to identify challenges, trends, and potential research gaps in this field. Furthermore, this review encompasses robotic systems designed for anatomically similar regions or exhibiting comparable structures to those intended for interventions in the liver and kidney. These systems, which have shown potential for application in this field, are discussed to explore possibilities within this domain. The review concludes by proposing future research directions in this area.

Digital Object Identifier 10.1109/MRA.2024.3409788

INTRODUCTION

Thanks to the liver and the kidney, which play a critical role in the detoxification of our blood and waste elimination [1], [2], our body can function efficiently. Cancer still represents one of the major threats to our health, and it can significantly affect the life span of both our liver and kidney. According to the International Agency for Research on Cancer, liver cancer is the second-deadliest cancer worldwide [3]. Similarly, kidney cancer is the 16th-most-common cancer [4].

1070-9932/24©2024IEEE

Typically, clinicians rely on CT, MRI, and ultrasound (US) to examine hepatic and renal tumors [5], [6], [7], [8]. Among these imaging modalities, MRI can provide excellent soft tissue contrast [9], [10] while relying on nonionizing radiation, completely removing radiation exposure for both the clinician and the patient. Moreover, it enables clear visualization of the margins of the targeted tumor. In addition, the benefits of MRI are considerable in multiangle imaging and intraoperative monitoring of tissue, especially in cryotherapy [11].

In the context of tumor diagnosis and treatment, percutaneous needle biopsy stands as the gold standard [12] and is a well-established procedure for acquiring samples to confirm diagnoses following initial imaging, and percutaneous needle probes are typically used for treatment [13]. MRI-guided biopsy and treatment have been extensively investigated [14], [15], [16]. However, due to the smaller bore of these machines compared to CT scans and the higher imaging cost, their adoption for this application is still limited. Image-guided ablation methods, such as radio-frequency ablation (RFA), cryoablation, and microwave ablation, are robust interventional approaches for treating liver and kidney neoplasms [17], [18]. In comparison to open and laparoscopic surgery, percutaneous ablation provides a significantly less invasive approach and has lower morbidity and mortality rates [19], [20]. This should significantly shorten the postoperative recovery time of patients, minimize surgical discomforts and complications, and enhance the overall quality of patients' postoperative life.

As depicted in Figure 1, the percutaneous needle biopsy and ablation process generally involves puncturing the skin with a needle to reach the desired location under the guidance of medical images, enabling the surgeon to perform surgical interventions [21], [22]. However, this process can be quite time-consuming, especially for cryoablation, and the duration of the intervention depends on the experience of the operator [23]. Navigating the needle away from vital organs and blood vessels, ensuring precision in puncture location, achieving accurate targeted tissue positioning in real time, and ensuring efficacy within the treatment area are all challenges typically encountered by surgeons during surgical procedures. All these factors influence the overall success of the surgery.

Robotic needle insertion devices have been specifically designed to address the challenges related to inserting, navigating, and steering needles within the tissue surrounding the target anatomy within the body of the patient, within the confined space of the bore of the MRI scanner. These robots can act as interventional surgeons to drive and insert the needle into the lesions. As detailed in [24], robot-assisted needle insertion for tumor treatment offers potential advantages, particularly in accuracy for out-of-plane procedures, defined as instances where the needle is inserted at angles of 5° or more away from the axial or transverse plane, i.e., the anatomical plane defining the section view in Figure 2(b). Additionally, these interventions reduce repositioning time, indicating the substantial impact of robotic systems in oncology. Nonetheless, MRI-guided interventions still face numerous challenges [25], e.g., in the structural design of the robot, in the performance of MRI-compatible components and actuators, and in enabling real-time image-guided navigation, position/pose sensing, and estimation of the robot.

Previous reviews have covered MRI-compatible actuators, needle-based interventions, and MRI-compatible robotic systems [25], [26], [27]. However, a systematic review specifically focusing on MRI-guided needle insertion robots for the liver and kidney is not available. The complex anatomical features

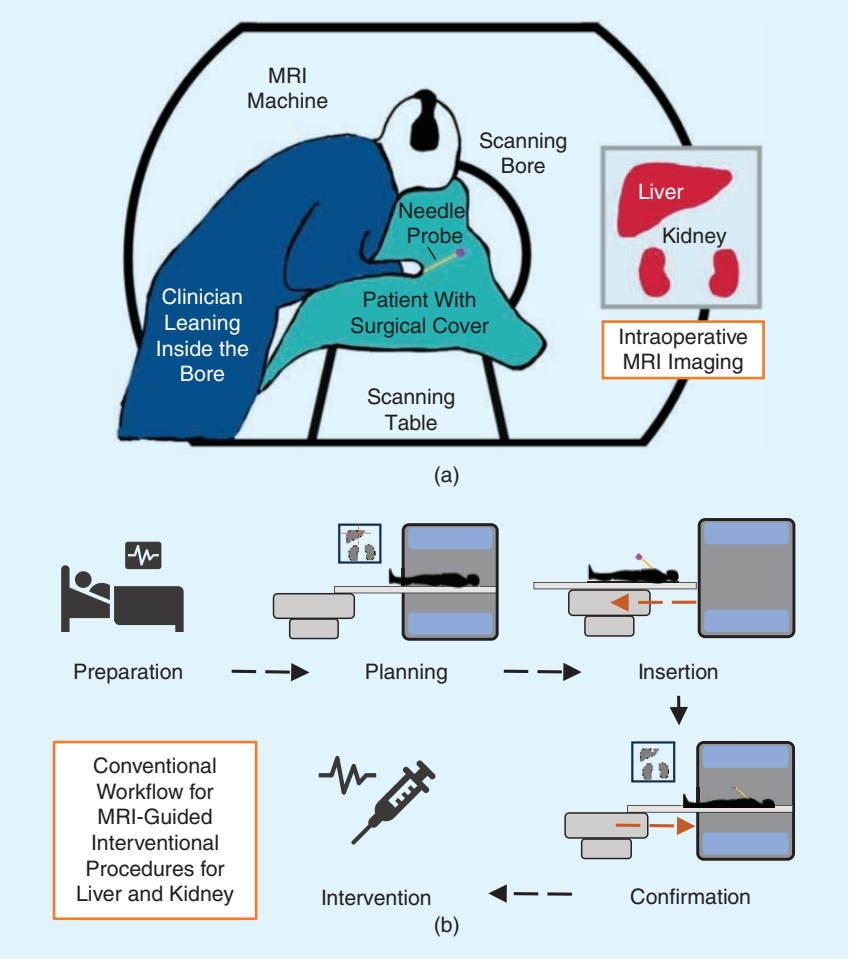

FIGURE 1. Typical scenario of MRI-guided interventions for liver and kidney. (a) Interventional MRI-guided procedures relying on insertion and steering of a needle-shaped probe to target anatomies inside the liver and the kidney under. (b): Conventional clinical workflow during the interventions.

and diversity of interventional approaches for both of them, particularly concerning tumor treatments, present an opportunity to collectively examine robotic systems targeted at these organs [28].

The distinct anatomical features and interventional challenges that differentiate liver and kidney procedures from those targeting other organs can be summarized as these three points:

1) The intricate anatomy of the liver and kidney poses significant challenges during interventions, particularly due to their complex tissue structure, high vascularization, and individual anatomical variations. Factors such as the numerous hepatic lobes; intricate network of bile ducts, veins, and arteries; and perinephric fat distribution, among others, add to the complexity. Additionally, the presence of the rib cage and adjacent skeletal and organ structures may further complicate procedures [28], [29], [30], [31], [32], [33].
2) The volume occupied by the robot within the confined MRI scanning bore needs to be carefully considered when targeting liver and kidney procedures. Typically, the main frame/structure of the robot should be positioned within the MRI scanner alongside the patient to facilitate needle insertion under real-time MRI guidance, ensuring that the inserted needle remains within the scanning bore [34], [35], [36], [37], [38]. The potential collision risk between the needle/robot and the narrow confines of the MRI scanning bore is a notable concern, especially considering the small diameter of the bore. Balancing between ensuring ample workspace for the robot to perform needle insertion and minimizing the robot's footprint within the MRI scanning bore presents a considerable design challenge. Hence, reducing the volume and weight of the robot while guaranteeing adequate workspace for seamless needle insertion remains a challenging task.
3) Addressing the impact of respiratory motion and organ movement on interventions involving the liver and kidney is also a crucial aspect [28], [29], [30], [31]. Both the liver and kidney are susceptible to substantial respiratory motion, potentially compromising the precision of interventions [28]. Furthermore, the motion induced by breathing can introduce artifacts in MRI images, affecting accurate diagnosis [39]. Therefore, considering motion compensation techniques during these interventions becomes imperative.

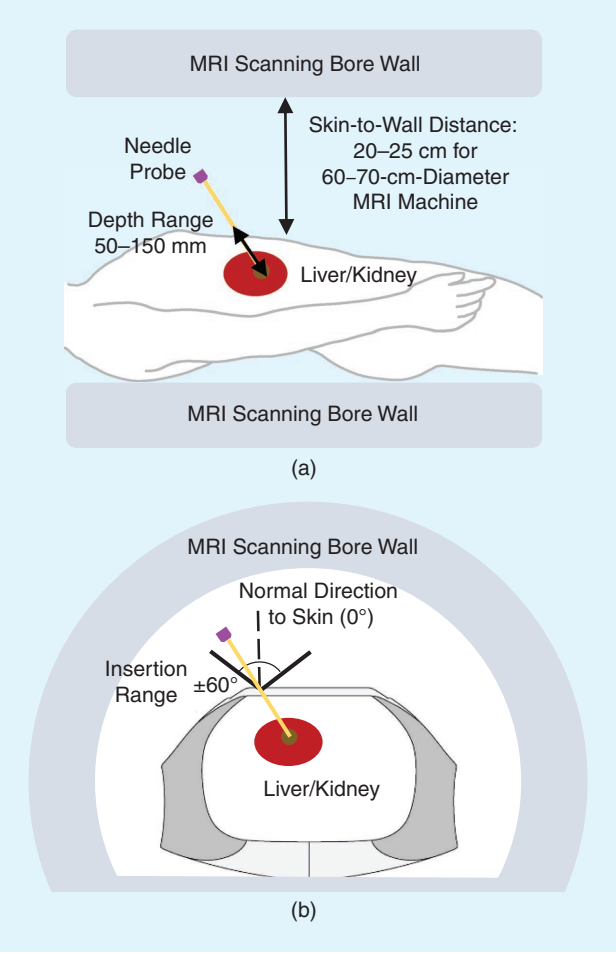

FIGURE 2. The workspace of interventional robotic systems for the liver and the kidney. (a) A side view of the patient body inside the MRI bore. (b) A section view of the body of the patient in the axial/transverse plane.

In this article, we aim to systematically review such systems, evaluating their robotic architecture, sensing, and control as well as exploring potential future prospects for these robots.

MATERIALS SELECTION

Google Scholar was chosen as the primary online source for this review, due to its extensive database and proven effectiveness in facilitating research efforts of this nature [26], [40]. The search string that was used to gather relevant literature in Google Scholar is presented in Figure 3. The Preferred Reporting Items for Systematic Reviews and Meta-Analyses method was utilized during the searching and filtering of the publications.

The search, conducted in July 2023, yielded 1,260 publications. Despite utilizing specific search terms, the results encompassed materials beyond the intended scope, including robotic systems for the prostate and non-English publications. To refine the selection, exclusion criteria were established to filter out materials that did not align with the focus of this review from the search results database. The following exclusion criteria are applied in this review:

1) *Non-English materials*: materials primarily written in languages other than English
2) *Other publication formats*: books, publisher indexes, meeting agendas, abstracts, conference proceedings, workshops, and so on
3) *Results without a link in Google Scholar*: citation-only items, i.e., items marked as [citation]; the source article of those items cannot be found in Google Scholar
4) *Other medical imaging modalities and applications*: CT, US, endoscopic and laparoscopic surgery, and so on
5) *Theses*: Ph.D. theses and dissertations of bachelor's and master's students

6) *Review articles*: articles summarizing the status of robotic systems, state-of-the-art summaries, editorial pieces, and so on
7) *Other organs/areas with limited potential for targeting liver and kidney*: targeted prostate, breast, and so on
8) *Other aspects*: works related to percutaneous intervention/minimally invasive surgery and those not focusing on needle insertion robots, including but not limited to needle-steering algorithms, technological principles of RF ablation, application of virtual reality/augmented reality (AR)/mixed reality in surgery, human–robot visual interface, trajectory planning of the needle, and so on.

During the process of reviewing the remaining materials, it was observed that certain items, although not directly related to the liver and kidney, still presented potential applications under MRI guidance. These robots were included in the review, as they shared similar applied regions, such as robotic devices focused on the trunk. Furthermore, in comparison to the prostate or other body parts, there has been a significant shortage of robots specifically designed for targeting the liver and kidney [41]. This highlights the challenges faced by both the research community and the industry in developing robots that meet the requirements for these procedures. Therefore, in addition to the primary objective of this review, which is to provide an overview of existing robots, the article also aims to shed light on innovative robots that have the potential to expand the possibilities for needle insertion in the liver and kidney. Robotic systems targeted at other organs/areas have been selected to explore potential robotic systems so that those robots can inspire researchers to develop suitable robots for liver and kidney applications. The following elaborates on the inclusion criteria for robots with potential applications in liver and kidney interventions. The proposed criteria are

1) *MRI-compatible robots*: These include robots targeting other anatomies in the trunk, such as the shoulder, lower back, and so on.
2) *MRI-compatible systems/devices for needle placement*: For these systems, specific target anatomy is not indicated, e.g., needle placement instruments and needle holders.
3) *MRI-compatible robots targeting anatomies outside the trunk*: These robots share similarities in structure or workspace with robots designed for liver and kidney interventions.

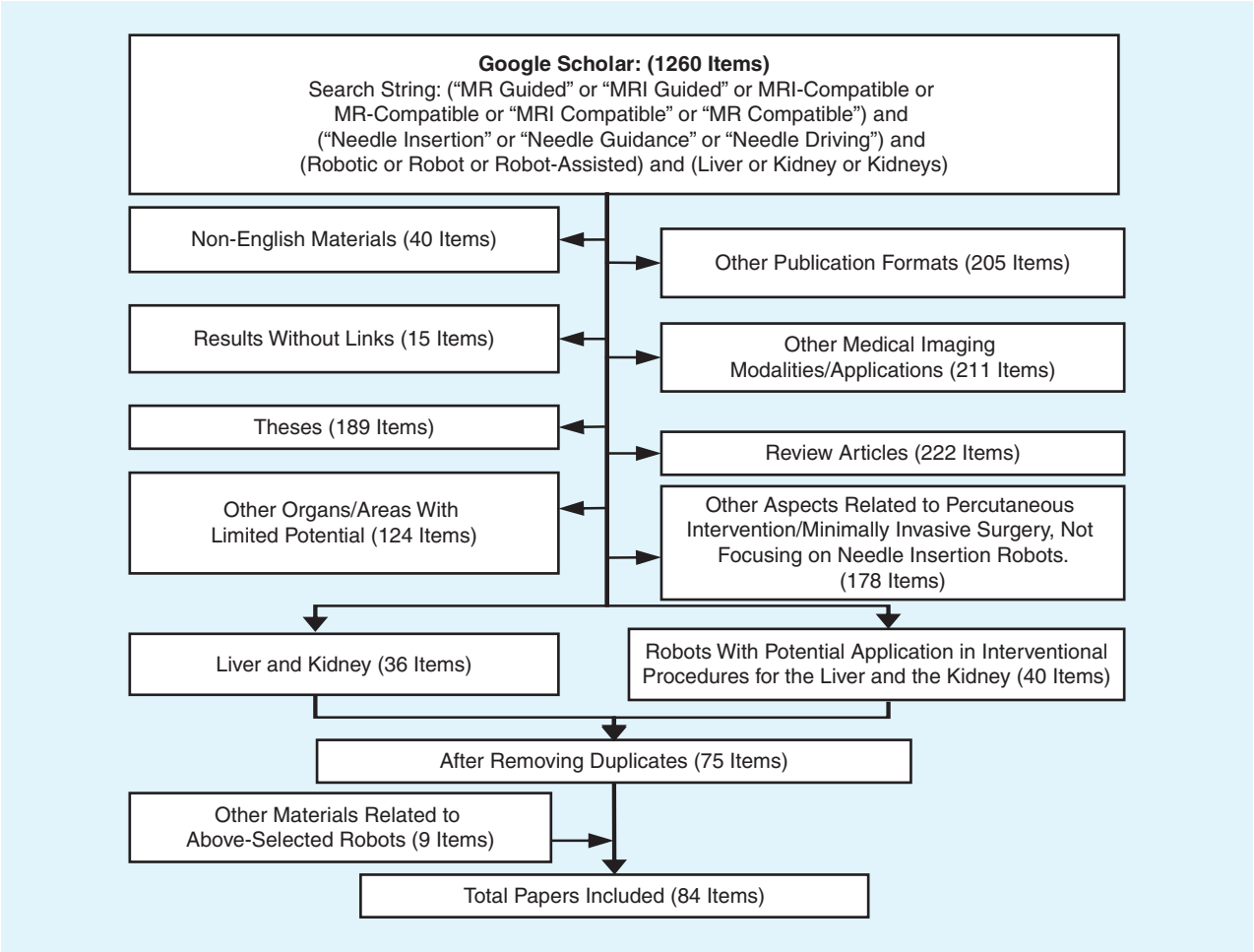

FIGURE 3. The Preferred Reporting Items for Systematic Reviews and Meta-Analyses process of material selection for the proposed systematic review.

4) *Non-MRI-compatible robots*: These robots share similarities in structure or workspace with robots designed for liver and kidney interventions, but either they are not MRI compatible or MRI compatibility is not explicitly indicated. Robots categorized into these groups might require minimal modifications to meet the requirements for liver and kidney interventions. Potential modifications may include adjusting the installation position of the robots within the MRI scanner; modifying auxiliary components, such as the positioning stage; or modifications in terms of materials to enable MRI compatibility.

After filtering the materials based on the proposed criteria, the remaining items were classified into MRI-compatible robots for interventional procedures for the liver and kidney and robots with potential applications in interventional procedures for the liver and kidney. In total, 36 research items focusing on robotic systems designed to target the liver and the kidney were included in the first group, and 40 research items focusing on robotic systems with potential applications for the liver and the kidney were included in the second group. Finally, nine additional research items deemed directly relevant to the first group were included by analyzing the bibliography of the materials collected with each. After removing the only duplicate in the first group, this review includes a total of 84 research items, with 40 robots with the potential for liver and kidney procedures being discussed in a dedicated section.

In this review, we aim to present the most up-to-date information about a large set of MRI-compatible robotic systems for percutaneous interventions. Information pertaining to the same robotic system from multiple publications has also been summarized in Tables 1–5. These tables provide a consolidated overview of the key details and advancements of each robotic system, allowing readers to gain a comprehensive understanding of the components of those robotic systems and capabilities. The "Structure" column in each table summarizes the kinematic chain of the robot using a synthetic notation, where "P" denotes a prismatic joint, "R" is a revolute joint, "S" means a spherical joint, and "U" represents a universal joint. When a paper provided a detailed kinematic diagram of the robot, we used this information to represent the kinematic chain using synthetic notation. In cases where detailed mechanical diagrams are lacking, the kinematic chain configurations have been inferred from CAD representations of the robotic systems to the best of the understanding of the authors. The "N/A" notation indicates challenges in ascertaining the kinematic chain of the robot based on available information in the papers.

CLINICAL AND TECHNICAL REQUIREMENTS FOR MRI-COMPATIBLE INTERVENTIONAL ROBOTIC SYSTEMS FOR LIVER AND KIDNEY

The liver and kidney are located within the abdominal cavity, with the liver occupying the upper mesoscopic region, while the left and right kidneys reside in the retroperitoneal region [42]. Quantitative and morphological analyses have provided insights into their average sizes, with the human liver being approximately 145.9 ± 29.8 mm in height, 196.1 ± 22.6 mm in diameter, and 86.2 ± 18.1 mm in thickness [43]. Anatomical and radiological studies showed that the left kidney is larger than the right [44]. Taking the left kidney as a reference, its average size is approximately 114.8 ± 7.2 mm in length, 54.2 ± 7.9 mm in width, and 47.6 ± 5.7 mm in depth [45]. MRI-guided percutaneous interventions have been employed for liver and kidney tumors using cryoablation [46] and microwave ablation [47]. The accuracy of needle operation, workspace, and puncture force should meet the medical demands when developing robot-assisted devices.

In terms of positional accuracy of the tip of the needle-shaped probes used in this procedure, a 3-mm error is deemed acceptable [10], [34]. Similarly, a questionnaire conducted at the 2018 Annual Meeting of the Cardiovascular and Interventional Radiology Society of Europe showed that the mean acceptable needle placement error was 2.7 mm [48], and comparative studies on CT-guided needle insertion showed that the error should be less than 3 mm [49]. In the context of interventional percutaneous procedures for tumor treatment, the safety margin should also be considered. A safety margin is the distance between the outer edge, or border, of the tumor and the volume of the tissue that clinicians aim to treat using either RFA, microwave ablation, cryoablation, or irreversible electroporation. This margin accounts for the additional tissue surrounding the tumor that needs to be included during the procedure to ensure the complete eradication or treatment of the tumor cells. [50], [51], [52]. Five to 10 mm is typically regarded as an acceptable range for the safety margin for liver and kidney interventions [53], [54], [55], [56].

Standard commercial interventional needles used in clinical practice for the liver and the kidney typically range from gauge G15 to G18, with a length that may differ for the same gauge based on the targeted anatomy [57], [58]. Various materials are used to enable MRI compatibility and ensure the robustness of the needle, such as chromium, ceramic, carbon fiber, titanium, steel, plastic, and glass fiber. In addition, the artifacts of needles made of different materials were also explored [59].

Sufficient puncture force needs to be applied to the needle(s) to penetrate the skin and the underlying tissue to reach the lesion site. In [60], it is reported that the maximum force applied during needle insertion into the liver when puncturing the skin is approximately 2 N, while in [61], the average maximum forces ranged from 2.75 to 2.8 N when targeting the kidney during in situ cadaveric studies. This difference is associated with different insertion depths, the type of needle probe used, and the insertion speed, thus resulting in different values of the maximum force [62], [63], [64].

In a randomized controlled experiment between robot-assisted and freehand needle positioning, the mean depth of hepatic tumors was 88.45 mm, with the maximum being 124.7 mm, and the average diameter of the tumor was 23.05 mm [24]. Similarly, a clinical review with 65 patients focusing on CT-guided percutaneous cryoablation for the treatment of renal tumors showed that the mean skin-to-tumor distance was around 76 mm, with an average diameter

TABLE 1. MRI-guided robots targeting the liver and kidney.

INSTITUTION	REFERENCE	TYPE	ACTUATOR	INSERTION	DOF	STRUCTURE (KINEMATIC CHAIN)	SENSING	CONTROL	START YEAR
UTokyo	[76], [77]	Table mounted	Ultrasonic	Manual	3	Sliding stage and five-bar linkage (P[5R]U-U)	Encoder, optical tracker	Control PC	2004
TIMC Lab	[34], [74], [82], [99], [100]	Body mounted	Pneumatic, piezoelectric	Robotic	5	Double-stage Cartesian gantry (2PRU-U2P)	Imaging, encoder	Imaging-based control, simple closed-loop control	2004
WUSTL	[89], [90], [91], [92]	Ground based	Ultrasonic, cable driven	Robotic	7	Cartesian gantry and arm (3P3RP)	Encoder	Man-in-the-loop control, leader–follower	2005
BWH, HMS	[86]	Ground based	Ultrasonic, passive	Manual	5	*XYZ* stage and arm (3P2R)	Encoder, optical-fiber sensors, optical tracker	RCM control	2005
	[85]	Ground based	Ultrasonic, passive	Manual	5	*XYZ* stage and arm (3P2R)	Encoder, optical-fiber sensors, optical tracker	Virtual human–machine interface control, RCM control	2008
	[10], [101], [102], [103], [104]	Body mounted	Passive, ultrasonic	Manual	2	Double rings (PRR)	Encoder, images	PID, motion compensation	2013
SUMS	[84]	Ground based	Ultrasonic, passive	Manual	5	*XYZ* stage and arm (3P2R)	Encoder, optical tracker	RCM control	2009
Chiba U	[78]	Ground based	Ultrasonic	Manual	16	Arms and two arms with RCM (14-DoF holding device + RPS-U)	Encoder, optical tracker	Control PC	2010
ATC, UCY	[35], [73], [93]	Table mounted	Passive, cable driven	Robotic	5	Arch-shaped component and beam (RPRRPP)	N/A	N/A	2012
MIT	[105]	Body mounted	Piezoelectric, cable driven	Manual	2	Sliding carriage on rotating arch (RP)	Encoder	PID	2013
ICL	[36], [67], [79], [80], [94]	Table mounted	Pneumatic	Manual	3, 4	Hybrid serial–parallel cylinder (2-PRPU)	Encoder, pressure sensor	SMC, high-level control strategy, time delay control	2014
	[111], [112], [121]	Needle driver	Pneumatic	Robotic	1	Leader–follower linear cylinder (P)	Optical force sensor, encoder	Time delay control, adaptive and predictive control	2015
UdeS	[81]	Body mounted	Pneumatic	N/A	4	Two-stage actuator (2-[3P]S)	DES	Stiffness control	2015
UDS	[87], [109]	Body mounted	Cable driven	Manual, robotic	3	Two helical-shaped compliant joints (RRP)	Encoder	Leader-follower	2015
	[113]	Needle driver	Pneumatic	Robotic	1	Auxetic structure and inchworm kinematics (N/A)	Pressure sensor	Pressure time control	2018
UF	[83]	Body mounted	Cable driven	Manual	2	Two movable plates (N/A)	Imaging	N/A	2019
HKU	[106]	Body mounted	Hydraulic	Manual	2	Cross arch and soft hydraulic actuator (2-RP)	Encoder	PID	2020
SU	[88], [96]	Table mounted	Hydrostatic, pneumatic	Robotic	7	Robotic arm (6RP)	N/A	Teleoperation	2020

(*Continued*)

TABLE 1. MRI-guided robots targeting the liver and kidney. (*Continued*)

INSTITUTION	REFERENCE	TYPE	ACTUATOR	INSERTION	DOF	STRUCTURE (KINEMATIC CHAIN)	SENSING	CONTROL	START YEAR
UArk	[37], [110]	Body mounted	Pneumatic	Robotic	6	Based on Stewart–Gough platform (6-UPS)	Encoder, pressure sensor	SMC	2021
UT	[38]	Body mounted	Pneumatic	Manual	4	Double stages ([2-PR]R)	N/A	Open-loop control	2022

UTokyo: University of Tokyo; TIMC Lab: TIMCL Laboratory; WUSTL: Washington University in St. Louis; BWH: Brigham and Women's Hospital; HMS: Harvard Medical School; SUMS: Shiga University of Medical Science; Chiba U: Chiba University; ATC: Ayios Therissos Center; UCY: University of Cyprus; MIT: Massachusetts Institute of Technology; ICL: Imperial College London; UdeS: University of Sherbrooke; UDS: University of Strasbourg; UF: University of Freiburg; HKU: University of Hong Kong; SU: Stanford University; UArk: University of Arkansas; UT: University of Twente; RCM: remote center of motion; PID: proportional-integral-derivative; P: prismatic joint; R: revolute joint; S: spherical joint; U: universal joint; N/A: not applicable or unclear in the material; SMC: sliding mode control; DES: dielectric elastomer sensor.

TABLE 2. MRI-guided robots targeting other anatomies in the trunk.

INSTITUTION	REFERENCE	TARGET	TYPE	ACTUATOR	INSERTION	DOF	STRUCTURE (KINEMATIC CHAIN)	SENSING	CONTROL	START YEAR
IGmbH, IMSaT, NIH	[127], [128], [129], [130]	Spine, heart	Table mounted	Ultrasonic, pneumatic	Robotic	6	Arch and beam (5P2R)	Limit switch, encoder	N/A	2003
WU	[146]	General	Table mounted	Ultrasonic	Robotic	4	Double SCARA-style arm (P5RS)	Encoder	N/A	2006
CNMC, AUSTB	[131], [132]	Shoulder	Body mounted	Piezoelectric	Manual	4	Circular base and sliding lifting bar (RP[4RU])	Encoder	N/A	2014
JHU	[137], [138], [139]	Shoulder, lower back	Body mounted	Piezoelectric	Manual	4	Circular base and scissor mechanism (2-6 R)	Encoder	Custom-developed control system	2017
	[133], [134], [135], [136]	Shoulder	Body mounted	Piezoelectric	Manual	4	Circular base and sliding lifting bar (RP[4RU])	Encoder	Galil motion controller	2018
	[140]	Lower back	Body mounted	Cable driven	Robotic	2	Beaded chain transmission (PR)	Encoder	Galil motion controller	2019
	[141], [142], [143], [144], [145]	Lowerback	Body mounted	Piezoelectric	Robotic	4, 6	Double-stage Cartesian base and needle driver ([2-PPU]PR)	Encoder	Galil motion controller	2020

IGmbH: Innomedic; IMSaT: Institute for Medical Science and Technology; NIH: National Institutes of Health; WU: Waseda University; CNMC: Children's National Medical Center; AUSTB: Azad University, Sough Tehran Branch; JHU: Johns Hopkins University.

of the tumor of approximately 24 mm [65]. In a CT-guided robotic system evaluation experiment on animals, the depth range of targets was 64–146 mm [49]. De Jong et al. investigated the clinical procedure scenarios of 365 needles used for thermal ablation of liver tumors in the period of 2008 to 2016 [66]. Their findings showed that around 90% of the needles had an insertion depth ranging between 50 and 150 mm, with an average depth of 95 mm. Moreover, the study indicated a mean needle deflection toward the target of 1.3 mm [66]. The typical depth range beneath the skin surface for the targeted tumors in these procedures was established and is illustrated in the schematic representation in Figure 2. Assuming that the perpendicular to the skin is 0°, the typical angular insertion range of a robot is ±45° [41], [67], and the range extending to 60° also holds clinical significance [36]. The maximum insertion angle in a robotic evaluation experiment for thermal ablation with 21 patients was around 60° [68]. This needle insertion angle was also observed in preclinical validation [69].

As certain sections of the liver and kidney lie beneath the rib cage, surgeons can adopt various needle insertion pathways, such as subcostal and intercostal routes, along with flexible patient positioning [29], [32], [70], [71]. Moreover, the orientation of the patient, whether headfirst or feetfirst inside the MRI machine, during surgery is a critical consideration. Given these factors, expanding the range to ±60° may accommodate a wider array of lesions and offer increased procedural convenience. However, it is important to note that the workspace of the needle can be affected by the position of the patient on the surgical table, and the insertion angle depends on the location of the biopsy site, on the position of the targeted tumor, and on the preferred trajectory determined by the surgeon.

The typical diameter of an MRI scanner ranges from 60 to 70 cm [72], and while machines with a bore of 80 cm exist, e.g., Magnetom Free.Max (Siemens Healthineers, Erlangen, Germany), they are not common in hospitals. While open-bore MRI machines are available in a limited number of clinics for medical examinations and interventions, closed-MRI machines are still prevalent in medical applications, due to their ability to generate higher magnetic fields, resulting in higher image quality. The small diameter of the bores of these machines, paired with depths ranging from 100 to 150 cm,

TABLE 3. MRI-guided robots for other types of needle placement.

INSTITUTION	REFERENCE	TARGET	TYPE	ACTUATOR	INSERTION	DOF	STRUCTURE (KINEMATIC CHAIN)	SENSING	CONTROL	START YEAR
ICT-CAS	[148]	N/A	N/A	N/A	Robotic	6	Base stage and half arch (2PR2P)	Position sensor	N/A	2011
UDS	[41]	N/A	Needle driver	Cable driven	N/A	2	Variable-stiffness tensegrity mechanism (4 R)	Encoder	Open-loop control	2015
	[149]	N/A	Needle driver	Cable driven	N/A	N/A	Variable-stiffness spherical joint (N/A)	N/A	N/A	2016
SIAT-CAS	[147]	N/A	N/A	Pneumatic	Robotic	5	Hybrid serial–parallel cylinder ([2-PRPU]P)	Laser distance sensor, pressure sensor	Fuzzy PID	2019

ICT-CAS: Institute of Computing Technology, Chinese Academy of Sciences; SIAT-CAS: Shenzhen Institutes of Advanced Technology, Chinese Academy of Sciences.

TABLE 4. MRI-guided robots targeting nontrunk anatomies.

INSTITUTION	REFERENCE	TARGET	TYPE	ACTUATOR	INSERTION	DOF	STRUCTURE (KINEMATIC CHAIN)	SENSING	CONTROL	START YEAR
UTokyo	[150], [151]	Neurosurgery	Table mounted	Ultrasonic	Robotic	6	*XYZ* base stage + arch (2PR2P)	Encoder	N/A	1995
BHU	[158], [159]	Neurosurgery	Table mounted	Ultrasonic	Manual	6	Delta mechanism (3-RRR)	N/A	Fuzzy tuning PD	2008
UH	[161]	Multiple (catheter system)	Body mounted	Cable driven	N/A	4	Circle base and two stages ([RPRRP]-[RRPR])	Encoder	Feedforward	2012
CNHS, JHU	[155], [156], [157]	Bone	Table mounted	Pneumatic	Manual	3	Arms and RCM linkage (arms + RP[8R])	Optical sensor	Image-guided control interface	2018
WPI	[152], [153]	Brain	Table mounted	Piezoelectric ultrasonic	Robotic	8	*XYZ* base stage and arch (3PU2PR)	Encoder	N/A	2020
NUS	[160]	Skull and so on	Body mounted	Cable driven	Manual	4	Two stages with sliders (2-RPS)	Encoder	PID	2020
GUT	[154]	Neurosurgery	N/A	Hydraulic	Manual	6	*XYZ* base, RCM linkage, and Scotch yoke mechanism (3PR[7R])	Encoder	N/A	2021

BHU: Beihang University; UH: University of Houston; CNHS: Children's National Health System; WPI: Worcester Polytechnic Institute; NUS: National University of Singapore; GUT: Guangdong University of Technology.

represents one of the main constraints to the introduction of interventional robotic systems that need to share the space inside the bore with the patient imaged. Taking the 60-cm MRI scanner as an example, the maximum distance between the wall of the gantry and the skin was estimated to be around 20 cm [73], with similar distances also measured in [74], offering a very limited workspace to any robotic system, especially in the case of patients with a higher body mass index. The diffusion of 70-cm-bore MRI machines opened new possibilities for the integration of robotic systems in MRI-guided interventional applications thanks to their larger bores [46]. Based on the above, the interventional workspaces for the liver and kidney are presented in the schematics of Figure 2. Additional challenges arise from the motion of the organs associated with the respiratory motion, which further complicates MRI image-guided procedures, considering the longer acquisition times required compared to CT imaging. As shown in [75], this displacement is the most significant in the craniocaudal direction for the liver. In this study, it reached up to 3.2 cm in free-breathing images and up to 4.4 cm in breath-hold images [75]. Therefore, the integration of breathing motion compensation both at the software and hardware levels becomes crucial for the development of efficient and effective MRI-guided robotic systems for interventional applications.

The recognized standard for medical devices in the MRI environment is ASTM F2503, titled *Standard Practice for Marking Medical Devices and Other Items for Safety in the Magnetic Resonance Environment*. This standard defines three distinct categories for devices used in MRI environments: MR safe, MR conditional, and MR unsafe. For a device to be labeled as MR safe, it must meet specific material requirements, including being electrically nonconductive, nonmetallic, and nonmagnetic. Conversely, MR-conditional devices demonstrate safety within defined conditions encompassing the static magnetic field, time-varying gradient magnetic fields, and RF fields. Compliance with the MR-safe standard is considered optimal for needle insertion robots in the MRI environment, given its stringent safety requirements. However, MR conditional serves as an alternative option since MR safe imposes more rigorous material demands on the components of the robots beyond mere nonmagnetic properties. Finally, MR unsafe denotes items that pose unacceptable risks to patients, medical staff, or others within the MR environment.

ARCHITECTURES OF MRI-COMPATIBLE ROBOTIC SYSTEMS FOR LIVER AND KIDNEY

The robotic systems identified in this systematic literature review can be classified based on the inclusion of one or both of the following subsystems: subsystem 1, a global/macropositioning frame, and subsystem 2, a needle-driving module [34], [76]. Subsystem 1 primarily focuses on positioning the needle in the desired location, while subsystem 2 is responsible for inserting and retracting the needle into/from the tissue. A complete MRI-compatible robotic system for the liver and kidney should embed both subsystems.

The publications included in this review are categorized according to the institution of the first author, and multiple classifications are proposed. Additionally, there are instances where different systems originate from the same institution.

As represented in Figure 4, the main classification is based on the mounting method employed by the proposed system: system 1, ground-based robot; system 2, table-mounted robot; system 3, body-mounted robot; and system 4, needle driver. Ground-based robots are installed permanently or temporarily on the floor beside the MRI scanning table during the intervention. Table-mounted robots are fixed on the scanning table and moved into the scanning area with the patient. Body-mounted robots are temporarily attached to the body of the patient during the procedure. Robots with an unspecified or unclear installation method are categorized as other frames, such as needle-driving modules.

In a common MRI-guided needle insertion intervention, as illustrated in Figure 1, the surgeon manually handles the needle and inserts it into the body of the patient under the

TABLE 5. Non-MRI-compatible robots with potential applications for the liver and kidney.

INSTITUTION	REFERENCE	TARGET	TYPE	ACTUATOR	INSERTION	DOF	STRUCTURE (KINEMATIC CHAIN)	SENSING	CONTROL	START YEAR
WU	[162]	Liver	N/A	DC motor	Robotic	3	SCARA-style arm (N/A)	Encoder	PID	2005
BIT	[163], [164]	Craniomaxillofacial surgery	Table mounted	Servo motor	Robotic	5	Arch gantry (N/A)	Encoder	PID and leader–follower	2018
UM	[165]	N/A	N/A	Cable driven	N/A	2	Two parallelogram arms with RCM ([5R] RP-[5R])	Encoder, force sensor	Tension distribution algorithm	2020
SDU	[166]	N/A	N/A	Cable driven	Robotic	2	Multiple pulleys with cables (N/A)	Encoder	N/A	2023

BIT: Beijing Institute of Technology, UM: University of Montpellier, SDU: Shandong University.

guidance of intraoperative MRI imaging. The imaging serves as feedback for the radiologists, enabling them to track the current location of the needle tip and steer it to reach the anatomical target. Figure 4(a) shows the different scenarios of robotic assistance based on the proposed classification according to the mounting location.

An additional level of classification is also introduced to differentiate between needle-steering modules based on a single- or a double-actuation stage, as in Figure 4(b). In double-stage systems, the needle is grasped at two different locations, resembling the manipulation performed by a surgeon using both hands. This approach enhances stability during the intervention, as demonstrated in systems presented in [36], [38], [76], [77], [78], [79], [80], [81], [82], and [83]. On the other hand, single-stage systems rely on a single grasping point to steer the needle, as seen in systems presented in [10], [84], [85], [86], [87], and [88]. This design architecture, although less robust, offers the advantage of being easier to implement and can make use of a straightforward structure like a rotation joint.

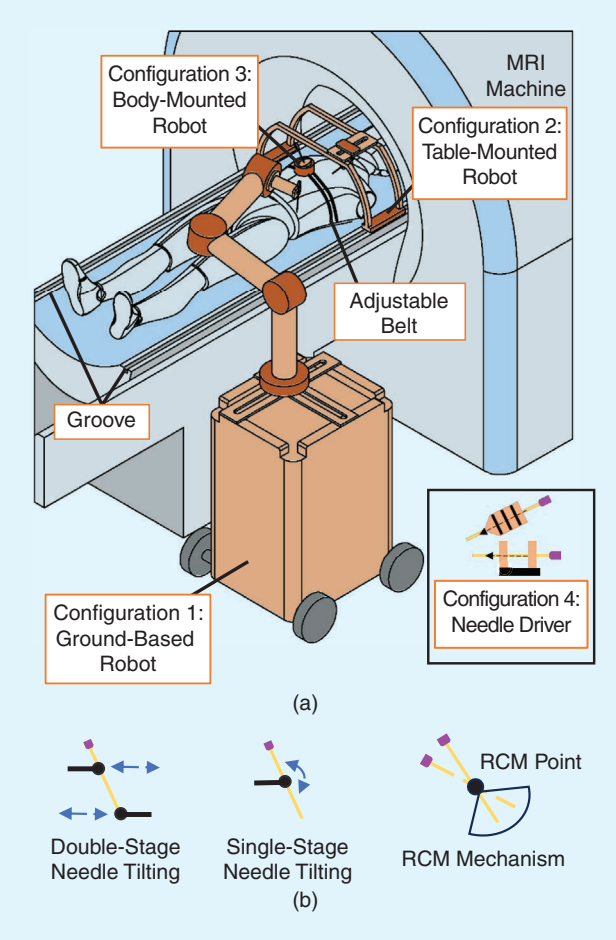

FIGURE 4. Robotic systems and needle drivers configurations (a) The four configurations for MRI-guided interventional robotic systems for needle insertion: configuration 1, ground-based robot; configuration 2, table-mounted robot; configuration 3, body-mounted robot; and configuration 4, needle driver. (b) Needle driver configurations to control needle tilting. RCM: remote center of motion.

Several robots used for skin puncture procedures do not integrate an actuator for needle insertion but only drive the needle holder to the targeted insertion point. This means that when completing the procedure, the surgeon needs to insert the needle manually through the needle holder instead of inserting the needle using a dedicated robotic actuator. Thus, the robot will be classified as a robotic needle driver if it embeds an actuation component for needle insertion or as manual insertion by the surgeon if it does not. This classification is used in the following sections and in Tables 1–5. The key features of the robotic system for the liver and kidney are summarized in Table 1.

GROUND-BASED ROBOTS

The obvious advantage of ground robots is their mobility in the crowded space surrounding interventional MRI machine-equipped theaters. This flexibility could potentially enable health-care facilities to adapt the robotic system to their specific needs and workflow requirements without the need for complex infrastructure modifications. This feature makes ground robots a practical choice for MRI-guided interventions, where space is often limited and the ability to maneuver around the patient and imaging equipment is crucial.

In the past, ground robots were developed for open-bore MRI [78], [84]. However, these systems are bulky compared to other types of robots for the closed-bore MRI, particularly body-mounted robots. Figure 5 describes the typical structure of a ground robot, which usually consists of a mobile base, a passive or active holder, and a needle-driving module [78], [84], [85], [86], [89], [90], [91], [92]. These ground robots typically rely on a Cartesian frame for their base. Lead screws actuated by US motors have been utilized in [84], [85], and [86] to enable the actuation of linear actuators associated with the Cartesian axis of the active base stages of these systems. The base stage is commonly positioned on one side of the MRI scanner.

Tsekos et al. developed a teleoperation robot with seven degrees of freedom (DoF) embedded in a Cartesian gantry

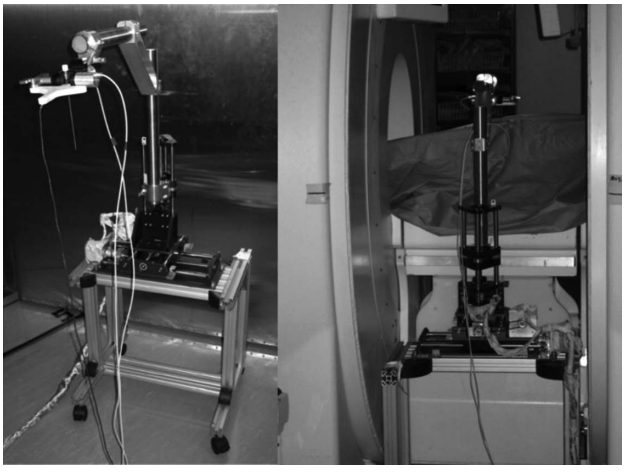

FIGURE 5. A typical bedside ground-based robot with a moving base and arms for an open-bore MRI machine [85]. (Source: Wiley-Liss; used with permission.)

system and multiple-DoF arms [89]. The arm joints are actuated through a series of shafts that span the entire length of the arm, interconnected by universal joints to facilitate the transmission [93]. In addition, the authors conducted a series of experiments to evaluate the performance of the robot and developed the GUI to form a mechatronic system [90], [91], [92].

Multijoint arms have also been explored for holding needle-driving stages, such as the 14-DoF system proposed by Sato et al. [78]. Passive designs incorporating gimbal mechanisms have also been proposed [86]. The combination of active and passive joints has been investigated in [78] to enable the creation of a remote center of motion (RCM) during needle steering. In addition, in order to achieve RCM motion at the end effector (EE), the Cartesian stage in the base allows for full control of the RCM position [86]. This RCM mechanism is explored in Figure 4(b), showing how different design configurations will result in different positions of the RCM of the needle.

Several mechanisms have been proposed to enhance the performance and safety of these systems during surgical procedures, especially during the treatment of tumoral tissue. This includes torque-limiting and height-constraining mechanisms, as seen in the system presented in [84]. Additionally, detachable needle adapters with predefined angles have been proposed in the same work to facilitate single-bedside operation.

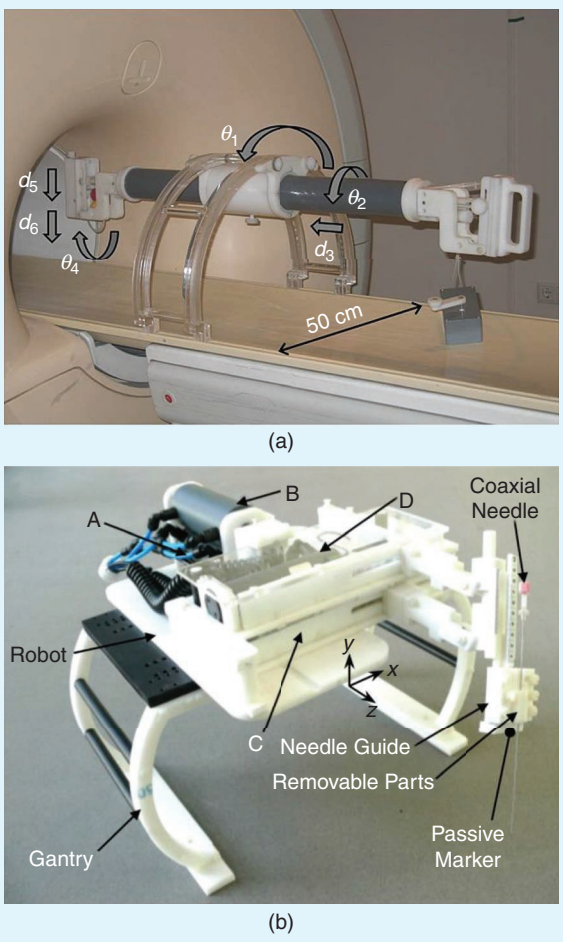

FIGURE 6. Typical table-mounted robots with an arch gantry. (a) A manually actuated table-mounted robot [93]. (b) A robot for MRI-guided liver ablation [80]. (Source: Wiley-Liss; used with permission.)

TABLE-MOUNTED ROBOTS

Differing from ground-based robots, table-mounted robots move together with the scanning table, hence, with the patient, even though some of these systems are also capable of overall relative motion with respect to the table. Thus, when the patient needs to be moved out of the scanning bore, the relative location of the robot with respect to the patient can easily be maintained constant. This design feature can enhance the repeated positioning accuracy of the robot. Furthermore, many of these systems utilize the rails running along the MRI machine table, which are typically used for scanner accessories, such as temporary coil installations, to enhance the imaging of specific anatomical targets. These rails facilitate the installation of the robot on the table. Two table-mounted robots [the robot proposed in [93] was installed using the table rails/groove in Figure 4(a)] are presented in Figure 6.

Some of the main challenges associated with table-mounted robots in MRI environments include the necessity for secure installation onto the MRI scanning table for interventions. Precise robot registration and sensing techniques are crucial for effective outcomes, particularly during patient repositioning. Rapid detachability from the table during surgery necessitates a structurally efficient solution. Managing the weight of the robot becomes crucial to avoid hindrance during installation, and collision avoidance with other medical instruments is essential due to its configuration on the scanning table.

Due to the cylindrical shape of the MRI machine bore, arched frames are preferred for table-mounted robots. The design challenges posed by the geometric and magnetic limitations of high-field MRI scanners were investigated by Keroglou et al. [35]. Based on this, Seimenis et al. proposed a 5-DoF robotic system optimized for such machines. This manipulator was subsequently used to investigate surgical planning in MRI-guided interventions, as presented in [73]. A prototype of the manually actuated robot was fabricated, embedding an arc support and a beam that carried a cable-driven needle-driving module, enabling the surgeon to insert the needle remotely [93].

An architecture that relies on a hybrid serial–parallel mechanism using pneumatic cylinders, one group on top of the other, which could also be used to achieve Cartesian movement, was explored by Franco et al. [36], [67], [79], [80], [94]. Two linear motors with differential movement in the same motion plane have been utilized to achieve rotation of one axis [36], [67], [79], [80], [94]. This approach offers a simple yet effective method to provide 2 DoF by employing differential motion in two directions [36], [80].

Table-mounted robotic systems with arm-based frames have also been explored. However, the strict electromagnetic

compatibility requirements specific to the MRI environment pose challenges for the use of commercial robot arms, including those robots utilized for CT-guided interventions, such as the system in [95]. Frishman et al. investigated the use of passive table-mounted arms to position the needle-driving module [96]. Later, in [88], they proposed an MRI-compatible 7-DoF robotic system with a 6-DoF arm based on hydrostatic actuation that used a rolling diaphragm hydrostatic system similar to the one they presented in [97]. They also proposed a two-way needle-driving module [96] to grasp, insert, and release the needle shaft to perform multistroke insertion. The clutch provided up to 25 N of force, which was sufficient for most interventions [96]. Frishman et al. demonstrated an integration of the needle-driving module, which the operator manipulates with a foot pedal valve [88].

Typically, these systems rely on MRI-compatible ultrasonic or piezoelectric motors as well as pneumatic, hydraulic, and cable-driven actuation. Hydraulic actuators offer reliable control of needle-driving modules [88], and they also enable the implementation of force feedback during the procedure [96]. In contrast, hydrostatic actuation, specifically using rolling diaphragms, is relatively uncommon, as exemplified in [97] and [98].

In open-bore MRI machines, design constraints are more relaxed, particularly for top–bottom-type machines, where table-mounted robots can be deployed without the strict space limitations inherent in closed-bore MRI systems. One proposed system for open-bore MRI environments is a needle placement robot with five links and a gimbal mechanism for needle tilting [76]. This robotic system was further enhanced by incorporating a translation stage at the base, allowing for an additional axial movement of 250 mm along the body of the patient axis to increase its reach across the entire liver volume [76].

BODY-MOUNTED ROBOTS

Body-mounted robots are systems fixed directly to the skin of patients, enabling the systems to move synchronously with the patients themselves. This unique feature allows for compensation of the respiratory movement during surgery, which can significantly affect the image quality in MRI-guided procedures, given their longer acquisition times, thus ensuring precise and accurate control [74]. Nevertheless, it is crucial to account for the weight of these robots and to ascertain the stability of their attachment to the skin of the patient. Ensuring this stability is imperative to avert any asynchronous movements between the robot and the underlying tissue. Such movements could adversely affect the precision and efficacy of the procedure as well as, more importantly, compromise the safety of the patient.

The light puncture robot (LPR) [99] serves as a typical example of a body-mounted robot. The system has undergone further development in subsequent studies [34], [82], where it incorporates a double-stage Cartesian needle-driving module. In double-stage systems, tilting of the needle is achieved by moving the two grasping points relatively in opposite directions. Besides the standard active Cartesian platform for macropositioning of the system, the early designs of the EE of the LPR included four straps connected to the needle to drive it toward the target [74], [99], [100]. A custom pneumatic actuator, inspired by clock making principles, consisting of a reciprocating piston rod and sprocket wheel, is introduced in these studies [74], [100]. The LPR robot was further improved to address various limitations, including issues related to sterilization, the support frame, and the performance of the custom pneumatic motors, aiming at improving the overall functionality and reliability of the system [34], [82]. In addition, later integrations focused on increasing the convenience of needle insertion and withdrawal and the detectability of the images [82]. The needle holder in the early system is a combination of a rigid lever arm and five passive joints, enabling rapid translation of the EE at a speed exceeding 9 cm/s [100].

Compact modular robotic systems, such as the Gantry-Mate [83], have also been investigated for MRI-compatible applications. This system consists of two movable plates that can be driven by a cable. The relative movement between the upper and lower plates enables needle tilting facilitated by the arms connected to each plate [83]. In addition, this robot was mounted on a macropositioning base platform, allowing for adjustments to be made during the procedure [83].

Double-ring mechanisms have been extensively investigated for body-mounted MRI-compatible interventional robots used in needle placement for kidney and liver applications [10], [101], [102], [103], [104]. One research team from Harvard Medical School proposed a double-ring mechanism for tilting the needle, which is suitable for common biopsies of liver and renal tumors [10], [104]. This robot has a small footprint and can be easily mounted on the abdomen skin of the patient inside an MRI machine bore [10]. Improved versions of this system can be found in [102], [103], and [104], as depicted in Figure 7. Furthermore, the accuracy assessment with motion compensation has been discussed in [103].

Arc structures, commonly used for table-mounted robots, have also been explored for body-mounted robots. In the work in [105], a cable-driven carriage sliding along an arc-shaped rail was utilized to adjust the orientation of the needle in one plane, and tilting the entire arc allowed for orientation adjustment in a second plane. This simple yet efficient mechanism provided a method to control the precise orientation of

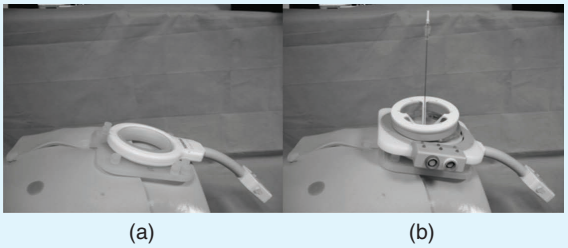

FIGURE 7. A typical body-mounted robot with a double-ring structure for needle insertion and a demonstration of deployment on a phantom torso [104]. (Source: Wiley-Liss; used with permission.)

the needle. Additionally, a latch mechanism was implemented to lock and release the needle, enabling sequential multineedle insertion. [105].

Researchers from the University of Hong Kong have developed a needle insertion robot utilizing soft actuation featuring two cross-semicircular arches [106]. This design shares similarities with the CT-guided SeeStar device [107] and enables precise needle insertion and manipulation. The portable needle robot has a diameter of 108 mm, a height of 115 mm, and a weight of 189 g. It achieves manual coarse adjustment, with a targeting error within 5°, through the use of two semicircular bridges, which serve as a macropositioning operation [106]. Additionally, the system utilizes three soft fluidic chambers and granular jamming to provide fine needle deflection, with an accuracy of 0.89 ± 0.31 mm, meeting the clinical requirements [106].

The soft robot has also been explored by Bouliane-Blais and Plante. The location of the needle can be adjusted using three artificial muscles arranged in a circular array [81]. Furthermore, the system incorporates granular jamming as a variable-stiffness mechanism, enabling a maximum stiffness of 7.7 N/mm, which is 19 times the initial value. This enhanced stiffness ensures that the needle remains in the targeted position securely [81]. Besides, the needle can be tilted around the axis when two of the three sets of independent pneumatic artificial muscles of two parallel stages move in different directions [81].

Wardhana et al. developed a double-stage 4-DoF robot with multiple needle insertions for irreversible electroporation to treat tumors [38]. The multiple-needle holder ensured the parallel insertion of all the needles [38]. A similar double-stage structure to tilt the needle was also previously reported in [82], but the robot proposed by Wardhana et al. employed a rotational base.

Bruyas et al. proposed a robot with a unibody structure and utilized two helical shape-compliant (HSC) joints [108] to rotate the needle [87]. Pfeil et al. utilized a similar HSC joint in their robot [109]. In addition, they created a leader–follower system, and the surgeon can adjust the angle of each joint on the leader side using two knobs [109]. This system is suitable for use in multimodal imaging environments, such as CT, cone beam CT, and MRI [109]. Four suction cups were utilized to position the robot to the patient [109]. The above two robots shared similar arch-shaped architecture.

The use of a parallel Stewart–Gough platform has been investigated in the context of needle insertion, as shown in the work of Musa et al. in [110], where a 6-DoF pneumatic parallel robot is presented. Phantom experiments demonstrated that the average position accuracy was 1.2 ± 0.43 mm, and the orientation accuracy was 1.09 ± 0.57°, while experiments conducted inside the MRI scanner resulted in an accuracy of 1.68 ± 0.31 mm for positioning and 1.51 ± 0.32° for rotating the needle [37].

Beyond the architecture of the robot, the interfaces between the robot and the skin of the patient should not be overlooked since they represent a crucial design element of the body-mounted robot to fix it to the body. The fixation of the mount between the robot and the patient can significantly impact the stability of the robot during movement, thereby influencing the precision and safety of interventions. Typically, adjustable straps or belts serve as the common method to secure the robot to the body of the patient through the belt slot on the robot [34], [37], [38], [82], [83], [100], [101]. While this approach offers user-friendly and convenient features, its firmness may vary based on the position of the center of gravity of the robot and the tightness of the strap. Lowering the center of gravity of the robot and ensuring an even weight distribution may enhance stability. In addition to single-fixation methods, several robots provide more flexible options. Adhesive pads are also suitable as a form of anchorage [105], [106]. It is noteworthy that the robot developed by Kwok et al. [106] used two adhesive pads and fastening belts as fixation methods. Adhesive pads might be effective for temporary positioning to identify the desired needle insertion point, with subsequent reinforcement using straps.

NEEDLE DRIVERS

In this section, we discuss additional types of robots that were not classified in the previous sections. One such example is the leader–follower pneumatic system developed by Franco et al. for teleoperated interventions [111], [112]. A 1-DoF prototype was fabricated to carry out experiments and verify the control approach.

In addition, Pfeil et al. introduced a 3D-printed pneumatic needle driver with a diameter of 29.2 mm and a length of 40 mm, incorporating an inchworm mechanism [113]. Unlike [87], the system by Pfeil et al. [109] is capable of robotic needle insertion, as it integrates a needle actuator with another inchworm mechanism [114]. Therefore, those compact robotic needle drivers have the potential to be integrated into other robotic systems.

SENSING AND CONTROL

This section discusses the sensing and control approaches of the MRI-compatible robots targeted at the liver and kidney. Tables 1–5 detail the main sensing and control strategies of each robotic system.

SENSING METHODS

Obtaining the pose of the needle and the motion information of the robot is essential for ensuring safety during the intervention. The data collected from sensors can be used to guide the robot to the correct area. However, the choice of sensor materials presents a challenge due to the nonmagnetic requirements of MRI environments. It is necessary to carefully select and develop sensor materials that are compatible with MRI to meet the specific needs of the robotic system. In practical robotic applications, various task-specific sensing requirements have been identified, encompassing aspects such as robot joint positions, spatial location perception of the robot, and force feedback. Different sensing methods have been investigated based on the specific requirements of each task.

In the context of detecting the rotation angle or stroke of the actuator in a robotic joint, the use of an encoder is an effective and straightforward approach. However, in the MRI environment, the use of electrical encoders is unsuitable due to the close proximity of the robot to the MRI scanner and because electrical signals can interfere with the MRI imaging [86] and compromise the accuracy of the pose information collected. Therefore, in the MRI-guided medical environment, alternative sensing solutions that are MRI compatible need to be employed to obtain accurate pose information for the robotic system and its EE. Consequently, the optical encoder became the preferred choice, not only for early robots but also for the most recent ones [67], [76], [79], [80], [84], [86], [94], [101]. The optical encoder is typically placed directly on the joint to measure the rotation angle accurately. In addition, in some cases, linear encoders have been used to detect the location of pneumatic cylinders [79]. Typically, the accuracy of an optical encoder is high; e.g., in [106], the resolution for motor control was 0.044°. Additionally, the compact size of these sensors facilitates their integration into the robotic systems [106].

The ability of the robot to sense its position, including its spatial relation to the MRI machine and, most importantly, the position of the tip of the needle, is crucial for its effective integration into clinical settings. Optical trackers have also been used to obtain position information in MRI-guided insertion robots, particularly for intraoperative navigation for task space sensing. An example of such a system is the optical 3D tracking system Polaris (Northern Digital, Waterloo, ON, Canada), which has been used to establish the geometric relationship between the manipulator and the MRI scanner. The data collected by the control device can then be used to measure the coordinate systems of the MRI gantry, manipulator, and manipulator needle [78]. The average registration error using the Polaris navigation system was reported to be 0.19 mm, while the total error of the needle placement system ranged between 1.24 and 4.1 mm [77]. However, the use of tracking markers can lead to occlusion issues [115]. When the intervention marker is hidden, the process may be influenced, as the location of the robot is lost. Furthermore, the size of the optical tracking system makes it challenging to integrate into compact robots, such as body-mounted robots, in clinical practice. In addition to traditional sensors, Bouliane-Blais and Plante demonstrated the potential of using a dielectric elastomer sensor (DES) in this application [81]. The DES is integrated directly into the shaft of the needle to measure its pose. Unlike its actuation counterpart, the dielectric elastomer actuator, the DES utilizes a significantly lower voltage for its operation. However, it is important to note that there is a risk of separation between the dielectric elastomer layer and the electrodes in large deformations, which could potentially impact the performance of the system [116].

Imaging itself can be used to provide position feedback for these robotic systems [99], serving as an alternative to optical or magnetic localizers. The fundamental principle of MRI relies on the excitation of hydrogen nuclei within a magnetic field [117]. To enable pose estimation of needle guidance robotic systems, small MRI markers filled with substances such as water [99], oil [74], and diluted gadolinium chelate solution [100] have been explored as a cost-efficient and practical approach for obtaining pose information in the MRI environment. Similarly, the GantryMate system [83] incorporates a cylindrical passive needle guider that contains a contrast agent solution. This enables the needle guider to be visualized in MRI images, providing guidance and feedback during the needle insertion procedure. The pose of the needle holder can be obtained using a specific tracking sequence [118]. Those images, including the pose of the needle holder, have been constructed using a phase-only cross correlation (POCC) algorithm [118]. After that, the sequence automatically aligns the plane of subsequent imaging acquisition with the marker direction. The proposed approach is convenient for the surgeon, as it allows them to visualize the insertion angle instead of manually adjusting the direction of the MRI scan. However, the image artifacts of the needle can impact the reconstruction process of POCC [83], which could pose a significant challenge for multineedle insertion. The use of MRI-visible spherical markers has been explored in [101] to register the robot in the MRI image. A workflow for MRI-guided percutaneous cryoablation with fully automated algorithms is proposed to detect and register these fiducial markers, to enable insertion planning, device registration, and placement monitoring. Despite substantial advancements in spatial sensing technologies, the real-time determination of the tip of the needle position and orientation within an MRI setting continues to pose significant challenges. These challenges are primarily attributed to constraints such as the diminutive scale of the needle (real-time responsiveness at high refresh rates) and the influence of intense magnetic fields.

Force feedback can also be exploited to enhance the interaction between the robot and the operator, allowing the surgeon to sense insertion forces in the human–robot interaction task. Force feedback is a crucial aspect of teleoperated procedures for needle insertion robots, as surgeons need to sense the applied force to ensure safe and accurate interventions. In [97], a rolling diaphragm hydrostatic transmission is proposed to enable force feedback in the robotic system. However, one challenge with this system is the complete removal of air from the whole pneumatic line to maintain consistent pressure [88]. The systems described in [88] and [96] are fully human powered, meaning that all the power required for the system comes directly from the interaction of the surgeon with the user interface of the device. This setup allows the operator to provide the necessary force while also perceiving the applied force during the intervention. The experiment results demonstrated 1:1 force feedback capabilities, with only <5% differences between the input and output [96].

Additional sensing capabilities could enhance the operational efficiency of the system. For pneumatic-actuated robots, pressure feedback may not be strictly necessary but can serve as a valuable monitoring tool. Studies like [67] and [114] have incorporated pressure sensors to oversee the pneumatic pressure in the system during pneumatic actuation. Furthermore,

researchers employing pneumatic cylinders [36] have also integrated pressure sensors into their setups.

CONTROL STRATEGIES

The strong magnetic fields and limited space in MRI environments present significant challenges for interventional surgeons [119]. In general, the patient needs to be pulled out of the scanning bore to perform the needle insertion, followed by relocation to the inner part of the MRI scanning bore to detect the location of the needle [120]. This process is time-consuming and labor-intensive, which can negatively impact the overall efficiency of the intervention.

To address this issue, teleoperation is typically employed in robotic systems developed for this application. This approach allows the operator to control the needle from outside the bore or even from the control room of the machine, enabling more convenient and efficient needle insertion procedures [120]. A passive hydrostatic teleoperation device has been developed by Frishman et al. [88]. This system provides remote access while ensuring that the follower arm accurately replicates the motion and force exerted by the leader arm. The errors were around 0.3 mm for different path following tasks [88]. The tendon-driven method has also been explored to drive leader–follower systems [109]. The experimental test demonstrated that the mean distance to targets was 3.1 mm for robotic insertions [109]. In addition, Christoforou et al. have developed a leader–follower robot consisting of an articulated control device with encoders integrated into each joint [90]. This robotic system also included manual needle control, leader–follower manipulation, preoperative (stereotactic) planning, and dynamic updating of the imaging plane [90]. These four control modalities provide the surgeon with adaptable control over the robot, catering to the specific requirements of the surgery. A more advanced integration between a mechatronic system and an MRI scanner was presented in [92]. The performance of this system was also assessed in vitro in an interventional scenario [91]. A 3.2-mm accuracy was observed in the evaluation process [91]. Pneumatic actuation is also commonly employed to enable the teleoperation of MRI-compatible robotic systems. However, it is important to account for the friction associated with the moving parts of pneumatic circuits, as it can influence the potential integration of force feedback. To address this issue, an adaptive controller for pneumatically driven MRI-compatible robots was proposed in [111]. The maximum error was below 5 mm [111]. Additionally, a force feedback strategy was explored by impedance and admittance control based on time delay position control, and an adaptive friction compensation algorithm with one parameter adjustment for impedance control was also proposed [112]. The evaluation demonstrated that the tracking error on the follower unit was ≤1.3 mm [112]. Given that the long supply lines in pneumatic actuation would result in a delay in the input to the system, a discrete, adaptive, and predictive control with force and input influence was proposed and realized acceptable tracking accuracy (root-mean-square error = 0.74 mm) [121].

Several MRI-compatible robotic systems rely on simpler yet effective proportional-integral-derivative (PID) controllers [101], [105], [106] as well as on sliding mode control [67], another effective alternative control algorithm widely employed in the control of these systems. Those robots employed by the above controller could maintain errors below 3 mm in their set experimental tests [67], [105], [106]. The experimental results demonstrated that the robots met the requirements for the intervention.

Design features can also be exploited to mechanically implement control of the angle of the needle (such as the RCM), as in the system in [10], and the errors in the phantom targeting test are less than 6 mm [10]. Morikawa et al. developed an RCM implementation, which was achieved through a combination of optical angle sensors and 3-DoF Cartesian base stages [84]. This system employed a synergistic human–machine interface control strategy able to fix the position of the puncture point in space when the interventional radiologist changes the posture of the manipulator [84]. A similar RCM control strategy is achieved in [85] and [86]. Those systems could maintain the accuracy of the needle with an RCM mechanism around 1~3 mm [84], [85], [86].

In the context of robotic systems that utilize medical imaging as a "sensor" for real-time control, image-based control is also a viable option [99]. However, these methods typically rely on computationally heavy image processing algorithms to get the robot to the desired location [99]. Experiments demonstrated that the error was below 2 mm. However, the experiments were conducted under a CT image [99].

ROBOTS WITH POTENTIAL APPLICATIONS IN INTERVENTIONAL PROCEDURES FOR LIVER AND KIDNEY

In this section, we analyze the systems for needle insertion that we found in our search that do not target either the liver or the kidney but show potential for this application. This section focuses on the architecture, the sensing modalities, and the control approaches of these robots while providing insights into their potential use for the proposed application.

MRI-GUIDED ROBOTS TARGETING OTHER ANATOMIES IN THE TRUNK

In comparison to robotic systems targeted at other body parts, like the prostate and head, robots aimed at the liver and kidney often require complete insertion inside the MRI bore, positioned in close proximity to the targeted organs. This necessity arises from the location of the liver and kidney within the trunk of the patient, demanding the robot to be in closer proximity to the specific area during the procedure. Conversely, in common interventions, like those for the prostate [122], [123], [124] and breast [125], [126], the workspaces, especially regarding horizontal needle insertion, may vary from that required for the liver and kidney. Consequently, it might not be essential for the entire robot to enter the MRI scanning bore in these cases. As a result, robots specifically targeted for organs or body parts within the trunk were considered the most promising, as they share similar work

scenarios with those for the liver and kidney. These robots are discussed in the following, and their key features are listed in Table 2.

The first robot on this list is the INNOMOTION system [127], the first MRI-compatible robotic system for general percutaneous interventions that have been commercialized and utilized in various clinical applications, including cardiac interventions [128], [129]. Similarly, the Manipulator for Interventional Radiology device was the initial version of this robot, initially designed for the treatment of spinal diseases [130]. It featured an arch-shaped arm combined with a cantilever mechanism, allowing the surgeon to navigate this robotic system in the narrow space of the MRI bore [130]. Despite obtaining the Conformité Européenne marking in 2005, the INNOMOTION system has been discontinued [25].

A number of body-mounted robots that showed potential use for liver and kidney interventions were also proposed. Monfaredi et al. developed a 4-DoF body-mounted robot for shoulder arthrography [131], [132]. The structure, consisting of a four-link mechanism and a rotation stage in the base, could control two positional and two rotational DoF of the needle [131], [132]. After the initial implementation, this robot underwent further development, and the upgraded system is delivered in [133] and [134]. Evaluations were conducted on accuracy and clinical workflow [135], [136]. The workspace of these robots is a circular area with a maximum 100-mm-diameter circle, a maximum of ± 40 mm for translation, and a minimum of ± 45° for tilting the needle [131], [132], [133], [134], [135], [136]. This robotic system is examined in Figure 8. A parallel body-mounted robot with a scissor mechanism was presented, verified, and evaluated [137], [138], [139]. The upper and lower scissor mechanism can move along a circular base stage [137], [138], [139]. The insertion angle of the needle can be adjusted, and when two scissor stages move together, the needle can be translated into a circular workspace [137], [138], [139]. Additionally, the system in [133] and [139] can be paired with that in [140], a remotely actuated needle-driving device, to realize a full robotic needle insertion device. In [140], a novel cable-driven method that relies on bead chains is introduced. The beads engage with the inner tooth space of the sprocket, driving its rotation, and the screw-and-rail mechanism transforms these rotational motions into linear motion, driving the insertion of the needle [140]. The beaded chain transmission has also been integrated into a number of other robots [141], [142], [143]. The core structure of the base stage of these robots was utilized to design other robots for lumbar injection [144], [145]. These systems embed two identical Cartesian stages that can translate the needle along two axes with the ball joint, enabling needle tilting. The overall size of the robot is around 219 × 250 × 87 mm [145], and the height with the remote needle driver is around 265 mm [141]. This size allows the surgeon to conduct the intervention practicably.

Apart from the above robots designed specifically for needle insertion, an MRI-compatible manipulator developed for abdominal minimally invasive surgery is introduced in [146]. The system is designed to be used in combination with open-bore MRI machines. The authors focused on the integration of standard tools for general laparoscopic surgery, such as endoscopes, forceps, and graspers. The system embeds a parallel mechanism actuated by a timing belt to drive the joints for height adjustment.

MRI-GUIDED ROBOTS FOR OTHER TYPES OF NEEDLE PLACEMENT

In this section, we present the systems developed for general needle placement tasks that we found in our search and that exhibited potential for interventional applications in the liver and the kidney. The main features of these robots are summarized in Table 3.

Zhao et al. proposed a 5-DoF pneumatic robot specifically for needle puncture [147], as illustrated in Figure 9. The kinematic chain of this robot is similar to the one proposed by Franco et al. [36]. However, this robot provides automatic needle insertion through commercially available pneumatic cylinders. A hybrid fuzzy PID controller is proposed to control this robot for fine position control, with minimal overshoot and low settle time/steady state [147]. In [148], Xiang proposes a

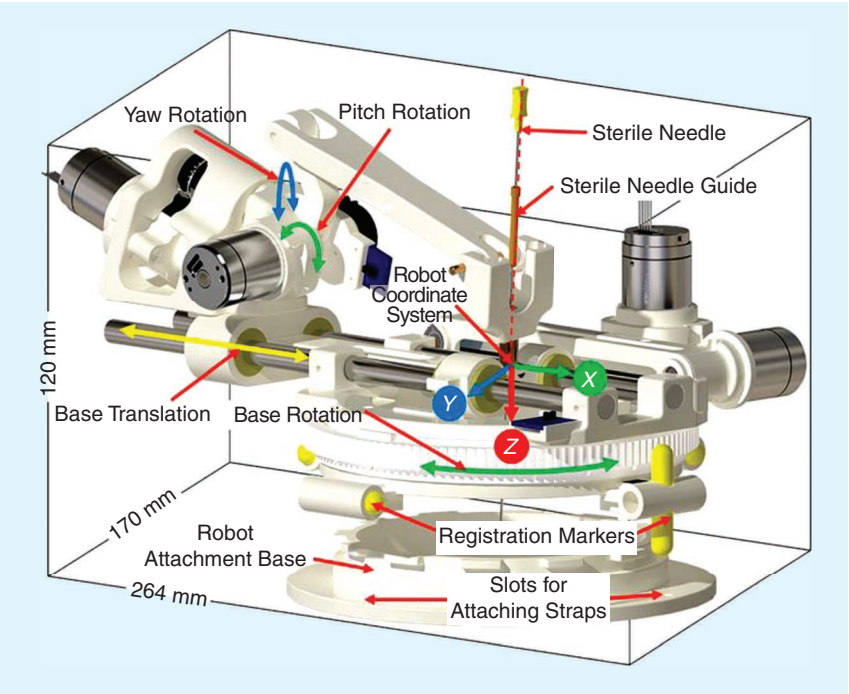

FIGURE 8. A potential robot for liver and kidney interventions, with a linkage for yaw and pitch and a circle base (targeted for shoulder arthrography). From [135]; used with permission.

localization framework with a transformation model based on thin-plate splines designed to operate a 6-DoF active needle holder in open-bore MRI environments to predict the position of the needle tip after deformation and to shift the coordinate from the MRI reference into the real-world reference.

Focusing on implementing compliance control in needle placement devices, Boehler et al. presented two systems based on the tensegrity principle: a parallel mechanism [41] and a spherical joint [149]. The system in [41] embeds a parallelogram tensegrity mechanism with a pair of tendons in series with spring elements to control the position of the kinematic chain and its stiffness. The system in [149] instead makes use of two elastic tendons for redundant actuation to control the position of the base of the system. Tensegrity is exploited in both devices to enable compliance control of the structure.

MRI-GUIDED ROBOTS TARGETING NONTRUNK ANATOMIES

The mechanical structures of needle insertion robots used in other body regions may differ from those designed for abdominal interventions, but they still hold potential due to their similarity in the workspace. For example, common features of robots designed for neurosurgical applications are the use of a Cartesian stage and quarter-arc structures [150], [151], [152], [153]. These robots offer Cartesian base stages that enable movement along the x-, y-, and z-axes, while the arc arm allows for needle tilting, which aligns with the requirements for liver and kidney procedures. Therefore, these existing structures could be adapted and contribute to advancements in liver and kidney interventions. In this section, such robots are discussed.

The same early examples of this kind of structure were proposed by the research team at the University of Tokyo back in 1995 [150], [151]. Since then, significant advancements have been made in terms of compactness, workspace, number of DoF, system integration, and performance of the driver module for these robotic systems. However, their fundamental design paradigm has remained largely unchanged. It is worth noting that while robotic systems originally developed for neurosurgical applications may show potential for interventional procedures in the liver and kidney, some adaptations may be necessary. For instance, their half-sided design may require adjustments in their mounting position on the patient table to accommodate the targeted anatomy.

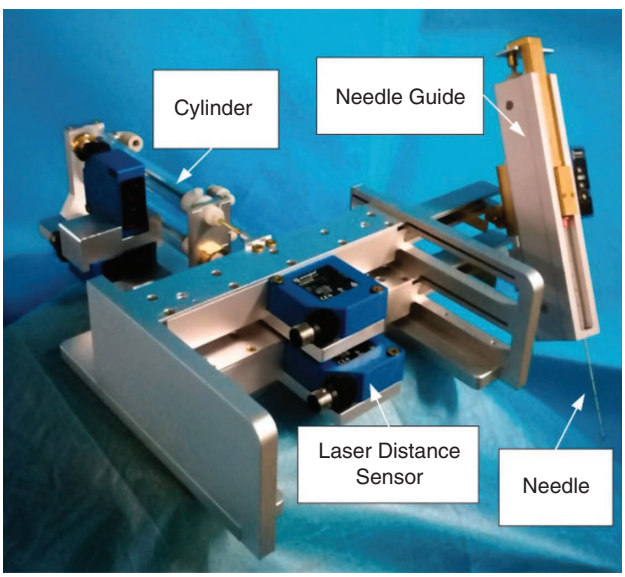

FIGURE 9. A robot for needle insertion with potential use in interventional applications for the liver and the kidney, embedding a serial–parallel structure [147]. (Source: Taylor & Francis; used with permission.)

Multilinkage mechanisms like the one presented in [154] also have the potential to be used in MRI-guided needle insertion, thanks also to their stable RCM implementation. Additionally, the team of Prof. Stoyanovici and Prof. Cleary at Johns Hopkins University developed a compact arm-based robot with a multiple-linkage RCM mechanism for MRI-guided bone biopsies [155], [156], [157]. This robot is actuated by a custom pneumatic stepper motor known as the PneuStep, which enables manipulation of the RCM linkage [157], clearly showing potential for the proposed application.

The use of delta platforms has also been investigated in the context of percutaneous interventions, as in the work of Hong et al., where the use of this mechanism has been explored in combination with a fuzzy controller [158], [159]. While this system shows potential for the proposed application, the integration of a gantry structure would be necessary to support its use in liver and kidney procedures.

When developing body-mounted robots, ensuring light weight and compactness is one of the main goals. Xiao et al. developed a portable robot that measures 40 mm in diameter and 45 mm in height [160]. The two-revolute, prismatic, and spherical (RPS) joint parallel needle positioner consisted of two prismatic stages that allow a slider to move along a linear rail [160]. In addition, these two stages can be rotated thanks to a revolute joint. The needle is inserted through the spherical joint of the slider on the two stages separately, allowing the needle to be tilted [160]. The system proposed in [160] shares a similar parallel architecture with the ROBOCATH system [161]. The former has been designed for the skull, while the latter has been developed for the orientation of surgical catheters. Given their designs, both systems have the potential for use in MRI environments for percutaneous interventions.

NON-MRI-COMPATIBLE ROBOTS WITH POTENTIAL APPLICATIONS FOR LIVER AND KIDNEY

In this final section, we present robotic devices that have the potential for application in percutaneous interventions for the liver and kidney. Unlike the devices discussed in the previous sections, these devices do not specifically address MRI compatibility. However, their designs hold promise for potential adaptation to an MRI environment. While they might require modifications to ensure MRI compatibility, their mechanical structures and control methodologies offer valuable insights for developing robotic systems tailored for liver and kidney interventions.

Kobayashi et al. introduced a manipulator [162] that incorporates force control, visual feedback, and organ model base control. This 3-DoF robot features three serial joints similar to a SCARA robot. The team conducted creep tests using ex vivo porcine models to assess the biomechanical characteristics of the tissue. This system shows promise for liver and kidney applications, especially considering its potential for force sensing and precise visual feedback during interventions.

Another relevant system with potential for liver and kidney applications is the 5-DoF robot presented in [163] and [164], designed for craniomaxillofacial surgery, as described in Figure 10. This robot can be considered a larger-scale version of the robotic system proposed by Wu et al. in [105], with evident similarities in the main structure. However, the 5-DoF robot offers augmented dexterity due to the additional DoF.

A 2-DoF tensegrity mechanism prototype, akin to the proposed RCM-based needle holder architecture in [41], is illustrated in [165]. By adopting the tendon-driven method utilized in it, this robot may become MRI compatible in the foreseeable future, expanding its potential for use in MRI-guided liver and kidney interventions. In addition, Li and Jiang introduced a tendon-driven puncturing surgical robot [166]. By introducing a decoupling mechanism embedding a movable pulley, they eliminate the influence of tendon coupling [166]. Providing that MRI compatibility is achieved, the system can be mounted on the arm, such as in [78], [88], and [96], to realize MRI-compatible needle insertion.

DISCUSSIONS AND CONCLUSIONS

According to the longitudinal review of existing robotic systems, it is evident that the architecture of these robots has evolved slowly over time. Many of the structures found in the early 21st century were already present in the previous century. This can be attributed to several possible reasons. The constrained space of the cylindrical closed-MRI scanning bore limits the choices for the main structure of the robot, leading to similar designs across different systems. As a result, Cartesian positioning base stages combined with orientation mechanisms have become a popular form for these robots. Additionally, the use of arc support in some robots represents an optimization to accommodate the circular bore of the MRI machine, enabling them to achieve an increased workspace, particularly for table-mounted robots. By contrast, open-bore MRI provides a large workspace for the structural design of robots. Indeed, MRI-compatible anthropomorphic designs (arm based) are not as common as Cartesian structures in these robotic systems. The open-chain design of anthropomorphic robots presents challenges in achieving a high level of stability, both in terms of actuation and the accuracy required at the EE.

The strict MRI compatibility requirements limit the use of standard high-performance electric actuators and sensors, which are commonly used in other robotic systems. Instead, ultrasonic and piezoelectric motors are often employed as alternative options for MRI-compatible robots. However, these motors can be expensive [27] and may not provide the same level of performance as electric actuators. Compact ultrasonic and piezoelectric actuators could become more popular choices for MRI-compatible robots, due to their great positioning accuracy and speed controllability, but their limited life span associated with RF shielding issues should not be overlooked [27], [167]. Additionally, fabricating and customizing these motors in laboratory environments can be challenging, further limiting their widespread use in MRI-compatible robotic systems [27]. Fluid-driven stepper motors, such as the PneuStep motor [168], the continuous motor developed by Dong et al. [164], and the pneumatic motor designed by Groenhuis et al. [169], have been embedded in different MRI-compatible robots [170], [171]. These motors show great potential to outperform both ultrasonic and piezoelectric motors at a fraction of the cost. However, these systems are still in the early stages of development, with most of the research being conducted in academic laboratories and only a few companies exploring their commercialization. As a result, their diffusion and integration into practical applications are limited. Unlike widely used MRI-compatible actuators, such as ultrasonic and piezoelectric actuators, hydraulic [106] and beaded chain transmission [140] methods have been relatively underutilized in MRI-compatible needle insertion robots. Hydrostatic approaches allow for the actuation unit to be relocated to the non-MRI-constrained environment of the control room while still providing satisfactory accuracy, especially for achieving fine position control as well as slow and smooth movement motion [172]. Additionally, hydrostatic actuators [88] could offer force feedback, enabling direct tactile feedback. Fluid leakage resulting in contaminants is a potential concern for these hydraulic systems [173]. In contrast, pneumatic motors may not face a similar issue, as their medium is typically air. However, maintaining stable high-pressure sources and consistent airflow is crucial for ensuring adequate torque. Furthermore, the use of long air pipes may introduce response delays [169].

An arch robot mounted on an MRI machine can indeed be a suitable structure that aligns with the circular scanning space. The arch design of the robot allows it to drive the needle holder efficiently while maintaining compatibility with the

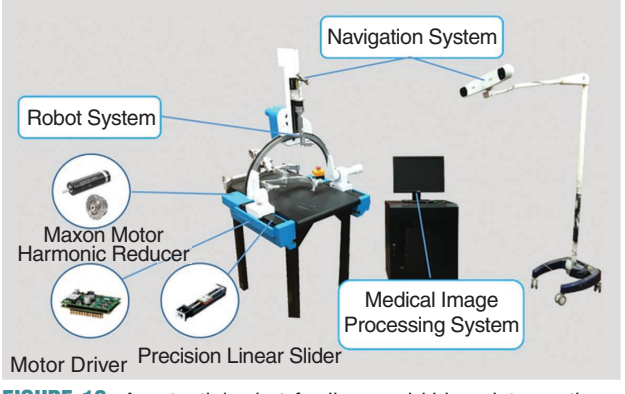

FIGURE 10. A potential robot for liver and kidney interventions, with an arch gantry (a non-MRI-compatible robot) From [163]; used with permission.

MRI environment. Due to its circular shape, this arch needle insertion robot is expected to offer a larger workspace compared to a robot with a top platform, which may have limitations in fully utilizing the circular bore of the MRI machine. The arch-extended workspace of the robot provides advantages in maneuvering the needle and allows for precise and versatile needle insertion during interventions.

Compact body-mounted robots are gaining popularity for needle insertion, offering the advantage of self-physical motion compensation in sync with patient respiration. However, achieving a balance between lightweight design and functionality, especially for multiple-needle insertion, remains a challenge. Ensuring a sufficient workspace while maintaining compactness is crucial. Additionally, stable fixation on the skin of the patient is vital. Inadequate attachment can cause the robot to lose strength and stability, particularly with long needle drivers. Proper fixation mechanisms are necessary to prevent undesired movements during interventions. Balancing compactness, stability, and functionality is crucial in developing effective body-mounted needle insertion robots for liver and kidney procedures. Ongoing research and advancements in design and materials hold promise for improving performance and usability in clinical applications.

The Cartesian frame has proven advantageous in pick-and-place applications, offering benefits such as a wide workspace, good reachability, simplicity, and predictability [174]. These advantages can be relevant for needle insertion robots as well, where tasks involve accurately grabbing the needle and precisely puncturing specific locations. The versatility of such robots would be highly beneficial if they could be utilized for multiple organs. However, some robots may be specifically designed to target particular organs or areas, tailoring their functionality for specialized procedures.

The number of DoF in robotic systems for liver and kidney interventions can significantly differ based on their types. For instance, compact body-mounted robots may effectively use two DoF to tilt the needle in two directions, owing to their small footprint, enabling manual positioning at specific needle insertion points. However, body-mounted robots may also integrate macropositioning frames, such as Cartesian frames with two translational DoF, to expand their workspace. On the other hand, table-mounted or ground-based robots, not in direct contact with the body, should ideally include 2- or 3-DoF positioning components to guide the needle to the intended insertion point, followed by a 2-DoF needle-tilting platform to alter its orientation. Usually, the needle driver has a single DoF for needle insertion. Yet, some needle drivers include an additional twisting DoF, aiding in manipulating the needle for flexible trajectory adjustments. This additional DoF allows for maneuvering the needle around significant anatomical structures by leveraging various needle tip geometries, facilitating navigation during interventions.

The RCM has been widely implemented in several medical robots for minimally invasive surgery. Wang et al. explored the application of this design feature in needle-based interventions, and their proposed mechanics-based model could aid in determining the optimal RCM location for needle-based interventions. [175]. As for the needle insertion robots targeting liver and kidney interventions, several robots considered this mechanism [10], [41], [76], [84], [85], [87], [101], [105], [106], [109], [160], [165]. Arch-shaped or circular components prove to be efficient and straightforward when implementing the structural design for the RCM mechanism, particularly for a body-mounted robot. These components secure the needle, allowing movement along the arch or ring, thereby enabling the rotation of the needle around the central point of the arch, i.e., the RCM. The double-stage rotation method in Figure 4(b) shows potential for achieving partial or complete RCM motion with ease.

Beyond traditional robotic design paradigms, soft robots show promise for MRI-compatible needle insertion applications. While their elastic properties may degrade over time, making their life span and accuracy a challenge, their low cost often allows for the creation of disposable devices, where only the actuation unit needs reusability. The flexibility of soft robots, combined with their intrinsic MRI compatibility associated with the use of nonmagnetic materials, minimizes the impact on the image quality. Soft robots can be explored alone or in conjunction with rigid systems to improve the performance of MRI-compatible robotic systems for the targeted application. Addressing the challenges associated with the durability and sterilization of soft robots could further enhance their potential in interventional procedures.

The strong magnetic field of MRI machines can pose material limitations for robots. Nonmagnetic metallic materials with exceptional mechanical properties can be used to fabricate these robots, such as aluminum alloys and brass. However, the MRI-safe standard in ASTM F2503 mandates the use of nonconductive, nonmetallic, and nonmagnetic materials for medical devices in MRI settings. Meeting these stringent requirements might prompt the cautious use of metal materials. However, the structural strength of these robots can be compromised by the use of nonmetallic materials. Polyether ether ketone and other high-strength plastics have shown good potential as materials for MRI-compatible needle insertion robots [176]. In addition, the MRI visibility of materials might be taken into consideration for several components, such as the needle. The robot also needs to be registered into the MRI image for localization. Thus, a comprehensive evaluation, balancing MRI safety, visibility, and mechanical performance, is crucial [177], and different materials are likely to be chosen for the different components of the robot.

The development of robotic systems for medical interventions is indeed influenced not only by advancements in robotics but also by improvements in medical imaging equipment. In the case of MRI-guided procedures, the loud noises generated by the MRI scanner can create a discomforting environment for both interventional surgeons and patients, even when earplugs are used. It is crucial to consider the noise level within the MRI suite as a critical design parameter when developing MRI-compatible robotic systems. Minimizing noise levels can contribute to a more comfortable and conducive environment for successful and efficient interventions, ensuring the best

possible experience for both patients and medical staff, further encouraging the adoption of these robotic systems, such as using teleoperation systems allowing surgeons to drive these robots remotely from the control room of the MRI scanner.

Despite significant advancements in MRI-compatible needle insertion robots for liver and kidney interventions, challenges persist in several key areas:

1) *Structural design*: There is a clear need to optimize the structural efficiency of the robot within the confined MRI scanning bore while ensuring adequate workspace coverage for the required organ areas during interventions.
2) *MRI-compatible components and actuators*: As robots transition from MRI compatibility to MR safety, material requirements extend beyond nonmagnetic properties, posing challenges to the structural stability of the robots. Actuators must meet various demands, such as precision, torque, speed, and size. Accessories like cables and pressure lines also demand assessment.
3) *Real-time image/assist navigation and planning*: Balancing image processing speed and quality is crucial. The impact of breathing-induced organ movement should be considered. Effective path planning and registration become critical in scenarios, especially for multineedle insertion. In addition, AR holds the potential to enhance the perception of surgeons as well as in the navigation and planning of MRI-guided interventions, such as [178]. Typical head-mounted AR devices [179] could be integrated into the teleoperating systems.
4) *Position/pose sensing and robot control*: This ensures precise and quick sensing of needle position/pose across different MRI sequences. Integration of sensors with robots to detect their status is essential for establishing a complete closed-loop control system.

In conclusion, the restricted cylindrical space of the MRI scanning bore has led to design similarities in the macroarchitecture of some robots designed for liver and kidney interventions. Among these, table-mounted and body-mounted robots have gained popularity. Although needle insertion robots have been developed for various applications, the number of specialized systems for liver and kidney procedures is still relatively limited compared to other parts of the body. However, the pressing clinical demand calls for potential solutions. Robotic systems equipped with real-time intraoperative MRI imaging can significantly assist surgeons during interventions, enabling more patients to receive precise and effective treatment. By providing improved visualization and precise needle placement, these robotic systems have the potential to save more lives and enhance the overall success rates of liver and kidney procedures. As technology continues to advance, it is expected that more innovative and MRI-compatible robots will be developed to address the unique challenges and complexities of interventions in the liver and kidney, further improving patient outcomes in the future.

ACKNOWLEDGMENT

This work was supported in whole or in part by the Wellcome/Engineering and Physical Sciences Research Council Center for Interventional and Surgical Sciences (Grant 203145/Z/16/Z) and the Royal Academy of Engineering, under the Chair in Emerging Technologies program (Grant CiET1819/2/36). Any opinions, findings and conclusions, or recommendations expressed in this article are those of the authors and do not necessarily reflect the views of the funders. For the purpose of open access, the authors have applied a CC BY public copyright license to any author-accepted manuscript version arising from this submission.

AUTHORS

Ziting Liang, Wellcome/Engineering and Physical Sciences Research Council Center for Interventional and Surgical Sciences, University College London, WC1E 6BT London, U.K. E-mail: ziting.liang.21@ucl.ac.uk.

Lukas Lindenroth, School of Biomedical Engineering and Imaging Sciences, King's College London, SE1 7EU London, U.K. E-mail: lukas.lindenroth@kcl.ac.uk.

Ryman Hashem, Wellcome/Engineering and Physical Sciences Research Council Center for Interventional and Surgical Sciences, University College London, WC1E 6BT London, U.K. E-mail: ryman_87@live.com.

Steve Bandula, Interventional Oncology Service, University College London Hospital, NW1 2BU London, U.K., and Wellcome/Engineering and Physical Sciences Research Council Center for Interventional and Surgical Sciences, University College London, WC1E 6BT London, U.K. E-mail: s.bandula@ucl.ac.uk.

Danail Stoyanov, Wellcome/Engineering and Physical Sciences Research Council Center for Interventional and Surgical Sciences, University College London, WC1E 6BT London, U.K. E-mail: danail.stoyanov@ucl.ac.uk.

Agostino Stilli, Wellcome/Engineering and Physical Sciences Research Council Center for Interventional and Surgical Sciences, University College London, WC1E 6BT London, U.K. E-mail: a.stilli@ucl.ac.uk.

REFERENCES

[1] C. G. Dielricli et al., "Influence of biliary cirrhosis on the detoxification and elimination of a food derived carcinogen," *Gut*, vol. 53, no. 12, pp. 1850–1855, Dec. 2004, doi: 10.1136/GUT.2003.037507.

[2] N. Wani and T. Pasha, "Laboratory tests of renal function," *Anaesthesia Intensive Care Med.*, vol. 22, no. 7, pp. 393–397, Jul. 2021, doi: 10.1016/J.MPAIC.2021.05.010.

[3] J. Ferlay et al., "Cancer statistics for the year 2020: An overview," *Int. J. Cancer*, vol. 149, no. 4, pp. 778–789, Aug. 2021, doi: 10.1002/ijc.33588.

[4] H. Sung et al., "Global cancer statistics 2020: GLOBOCAN estimates of incidence and mortality worldwide for 36 cancers in 185 countries," *CA Cancer J. Clin.*, vol. 71, no. 3, pp. 209–249, May 2021, doi: 10.3322/caac.21660.

[5] P. V. Nayantara, S. Kamath, K. N. Manjunath, and K. V. Rajagopal, "Computer-aided diagnosis of liver lesions using CT images: A systematic review," *Comput. Biol. Med.*, vol. 127, Dec. 2020, Art. no. 104035, doi: 10.1016/J.COMPBIOMED.2020.104035.

[6] C. Lopes Vendrami et al., "Differentiation of solid renal tumors with multiparametric MR imaging," *Radiographics*, vol. 37, no. 7, pp. 2026–2042, 2017, doi: 10.1148/rg.2017170039.

[7] K. H. Pan et al., "Diagnostic performance of contrast-enhanced ultrasound in renal cancer: A meta-analysis," *Frontiers Oncol.*, vol. 10, Art. no. 586949, Nov. 2020, doi: 10.3389/FONC.2020.586949/BIBTEX.

[8] M. R. Oliva and S. Saini, "Liver cancer imaging: Role of CT, MRI, US and PET," *Cancer Imag.*, vol. 4, no. Special Issue A, pp. S42–S46, 2004, doi: 10.1102/1470-7330.2004.0011.

[9] D. Ippolito et al., "Recent advances in non-invasive magnetic resonance imaging assessment of hepatocellular carcinoma," *World J. Gastroenterol.*, vol. 24, no. 23, Jun. 2018, Art. no. 2413, doi: 10.3748/WJG.V24.I23.2413.

[10] S. E. Song, J. Tokuda, K. Tuncali, A. Yamada, M. Torabi, and N. Hata, "Design evaluation of a double ring RCM mechanism for robotic needle guidance in MRI-guided liver interventions," in *Proc. IEEE Int. Conf. Intell. Robot. Syst.*, Tokyo, Japan, 2013, pp. 4078–4083, doi: 10.1109/IROS.2013.6696940.

[11] P. R. Morrison, S. G. Silverman, K. Tuncali, and S. Tatli, "MRI-guided cryotherapy," *J. Magn. Reson. Imag.*, vol. 27, no. 2, pp. 410–420, 2008, doi: 10.1002/jmri.21260.

[12] M. P. Curry and L. J. Jeffers, "Laboratory tests, noninvasive markers of fibrosis, liver biopsy, and laparoscopy," in *Schiff's Diseases of the Liver.* Hoboken, NJ, USA: Wiley, 2017, pp. 17–37, doi: 10.1002/9781119251316.ch2.

[13] F. Ridouani and G. Srimathveeravalli, "Percutaneous image-guided ablation: From techniques to treatments," *Press. Med.*, vol. 48, nos. 7–8, pp. e219–e231, 2019, doi: 10.1016/j.lpm.2019.06.005.

[14] M. Moche et al., "Navigated MRI-guided liver biopsies in a closed-bore scanner: Experience in 52 patients," *Eur. Radiol.*, vol. 26, no. 8, pp. 2462–2470, Aug. 2016, doi: 10.1007/S00330-015-4097-1/FIGURES/5.

[15] K. Ahrar et al., "Real-time MRI-guided cryoablation of small renal tumors at 1.5 T," *Investigative Radiol.*, vol. 48, no. 6, pp. 437, Jun. 2013, doi: 10.1097/RLI.0B013E31828027C2.

[16] R. L. Cazzato et al., "Diagnostic accuracy and safety of percutaneous MRI-guided biopsy of solid renal masses: Single-center results after 4.5 years," *Eur. Radiol.*, vol. 31, no. 2, pp. 580–590, Feb. 2021, doi: 10.1007/S00330-020-07160-6/TABLES/3.

[17] K. R. Kim and S. Thomas, "Complications of image-guided thermal ablation of liver and kidney neoplasms," *Seminars Interventional Radiol.*, vol. 31, no. 02, pp. 138–148, 2014, doi: 10.1055/S-0034-1373789/ID/JR00833-46.

[18] D. J. Breen and R. Lencioni, "Image-guided ablation of primary liver and renal tumours," *Nature Rev. Clin. Oncol.*, vol. 12, no. 3, pp. 175–186, 2015, doi: 10.1038/nrclinonc.2014.237.

[19] E. C. H. Lai and C. N. Tang, "Radiofrequency ablation versus hepatic resection for hepatocellular carcinoma within the Milan criteria—A comparative study," *Int. J. Surg.*, vol. 11, no. 1, pp. 77–80, Jan. 2013, doi: 10.1016/J.IJSU.2012.11.019.

[20] M. Aron and I. S. Gill, "Minimally invasive nephron-sparing surgery (MINSS) for renal tumours: Part II: Probe ablative therapy," *Eur. Urol.*, vol. 51, no. 2, pp. 348–357, Feb. 2007, doi: 10.1016/J.EURURO.2006.10.033.

[21] A. Veltri, I. Bargellini, L. Giorgi, P. A. M. S. Almeida, and O. Akhan, "CIRSE guidelines on percutaneous needle biopsy (PNB)," *Cardiovascular Interventional Radiol.*, vol. 40, no. 10, pp. 1501–1513, Oct. 2017, doi: 10.1007/s00270-017-1658-5.

[22] Y. Yan, Z. Y. Lin, and J. Chen, "Analysis of imaging-guided thermal ablation puncture routes for tumors of the hepatic caudate lobe," *J. Cancer Res. Therapeutics*, vol. 16, no. 2, pp. 258–262, Apr. 2020, doi: 10.4103/JCRT.JCRT_341_19.

[23] A. Caviezel, S. Terraz, F. Schmidlin, C. Becker, and C. E. Iselin, "Percutaneous cryoablation of small kidney tumours under magnetic resonance imaging guidance: Medium-term follow-up," *Scand. J. Urol. Nephrol.*, vol. 42, no. 5, pp. 412–416, 2008, doi: 10.1080/00365590801951632.

[24] W. J. Heerink et al., "Robotic versus freehand needle positioning in CT-guided ablation of liver tumors: A randomized controlled trial," *Radiology*, vol. 290, no. 3, pp. 826–832, 2019, doi: 10.1148/radiol.2018181698.

[25] N. Hata, P. Moreira, and G. Fischer, "Robotics in MRI-guided interventions," *Topics Magn. Reson. Imag.*, vol. 27, no. 1, pp. 19–23, Feb. 2018, doi: 10.1097/RMR.0000000000000159.

[26] R. Monfaredi, K. Cleary, and K. Sharma, "MRI robots for needle-based interventions: Systems and technology," *Ann. Biomed. Eng.*, vol. 46, no. 10, pp. 1479–1497, Oct. 2018, doi: 10.1007/S10439-018-2075-X/FIGURES/10.

[27] Q. Xiao, R. Monfaredi, M. Musa, K. Cleary, and Y. Chen, "MR-conditional actuations: A review," *Ann. Biomed. Eng.*, vol. 48, no. 12, pp. 2707–2733, Dec. 2020, doi: 10.1007/S10439-020-02597-8/FIGURES/24.

[28] N. Najmaei, K. Mostafavi, S. Shahbazi, and M. Azizian, "Image-guided techniques in renal and hepatic interventions," *Int. J. Med. Robot. Comput. Assisted Surg.*, vol. 9, no. 4, pp. 379–395, 2013, doi: 10.1002/rcs.1443.

[29] M. Seager, S. Kumar, E. Lim, G. Munneke, S. Bandula, and M. Walkden, "Renal cryoablation—A practical guide for interventional radiologists," *Br. J. Radiol.*, vol. 94, no. 1118, Feb. 2021, Art. no. 20200854, doi: 10.1259/bjr.20200854.

[30] C. Floridi et al., "Precision imaging guidance in the era of precision oncology: An update of imaging tools for interventional procedures," *J. Clin. Med.*, vol. 11, no. 14, 2022, Art. no. 4028, doi: 10.3390/jcm11144028.

[31] A. Granata et al., "Performing an ultrasound-guided percutaneous needle kidney biopsy: An up-to-date procedural review," *Diagnostics*, vol. 11, no. 12, pp. 1–13, 2021, doi: 10.3390/diagnostics11122186.

[32] G. Vijayaraghavan, S. David, M. Bermudez-Allende, and H. Sarwat, "Imaging-guided parenchymal liver biopsy: How we do it," *J. Clin. Imag. Sci.*, vol. 1, no. 1, pp. 1–8, 2011, doi: 10.4103/2156-7514.82082.

[33] S. Liu et al., "Automatic multiple-needle surgical planning of robotic-assisted microwave coagulation in large liver tumor therapy," *PLoS One*, vol. 11, no. 3, pp. 1–34, 2016, doi: 10.1371/journal.pone.0149482.

[34] N. Hungr, I. Bricault, P. Cinquin, and C. Fouard, "Design and validation of a CT-and MRI-guided robot for percutaneous needle procedures," *IEEE Trans. Robot.*, vol. 32, no. 4, pp. 973–987, Aug. 2016, doi: 10.1109/TRO.2016.2588884.

[35] C. Keroglou et al., "Design of MR-compatible robotic devices: Magnetic and geometric compatibility aspects," in *Proc. 9th Int. Conf. Inf. Technol. Appl. Biomed.*, Larnaka, Cyprus, 2009, pp. 1–4, doi: 10.1109/ITAB.2009.5394417.

[36] E. Franco, D. Brujic, M. Rea, W. M. Gedroyc, and M. Ristic, "Needle-guiding robot for laser ablation of liver tumors under MRI guidance," *IEEE/ASME Trans. Mechatron.*, vol. 21, no. 2, pp. 931–944, Apr. 2016, doi: 10.1109/TMECH.2015.2476556.

[37] M. Musa, S. Sengupta, and Y. Chen, "Design of a 6-DoF parallel robotic platform for MRI applications," *J. Med. Robot. Res.*, vol. 07, no. 02n03, pp. 1–12, Jun. 2022, doi: 10.1142/S2424905X22410057.

[38] G. Wardhana, Y. X. Mak, M. Abayazid, and J. J. Futterer, "Design and characterization of a multiple needle insertion MRI-guided robot for irreversible electroporation (IRE) treatment," in *Proc. 9th IEEE RAS/EMBS Int. Conf. Biomed. Robot. Biomechatron. (BioRob)*, Seoul, Korea, Republic of, 2022, pp. 1–6, doi: 10.1109/BioRob52689.2022.9925469.

[39] M. Honal, J. Leupold, S. Huff, T. Baumann, and U. Ludwig, "Compensation of breathing motion artifacts for MRI with continuously moving table," *Magn. Reson. Med.*, vol. 63, no. 3, pp. 701–712, 2010, doi: 10.1002/mrm.22162.

[40] N. R. Haddaway, A. M. Collins, D. Coughlin, and S. Kirk, "The role of google scholar in evidence reviews and its applicability to grey literature searching," *PLoS One*, vol. 10, no. 9, pp. 1–17, 2015, doi: 10.1371/journal.pone.0138237.

[41] Q. Boehler, A. Zompas, S. Abdelaziz, M. Vedrines, P. Poignet, and P. Renaud, "Experiments on a variable stiffness tensegrity mechanism for an MR-compatible needle holder," in *Proc. 5th Joint Workshop New Technol. Comput./Robot Assisted Surg. (CRAS)*, Bruxelles, Belgium, 2015.

[42] M. Scaglione et al., "A dissection's guide to human abdominal cavity," *EuroMediterranean Biomed. J.*, vol. 15, no. 18, pp. 36–39, 2020, doi: 10.3269/1970-5492.2020.15.8.

[43] A. C. Nagato et al., "Quantitative and morphological analyses of different types of human liver," *J. Morphol. Sci.*, vol. 28, no. 4, pp. 275–279, 2011.

[44] J. Frimann-Dahl, "Normal variations of the left kidney," *Acta Radiol.*, vol. 55, no. 3, pp. 207–216, 1961, doi: 10.3109/00016926109174541.

[45] D. Jovanović, B. Gasic, S. Pavlovic, and R. Naumovic, "Correlation of kidney size with kidney function and anthropometric parameters in healthy subjects and patients with chronic kidney diseases," *Renal Failure*, vol. 35, no. 6, pp. 896–900, Jul. 2013, doi: 10.3109/0886022X.2013.794683.

[46] R. L. Cazzato et al., "How to perform a routine cryoablation under MRI guidance," *Topics Magn. Reson. Imag.*, vol. 27, no. 1, pp. 33–38, Feb. 2018, doi: 10.1097/RMR.0000000000000158.

[47] Z. Li, D. C. Jiao, C. Wang, W. Zhang, J. Li, and X. Han, "MR-guided microwave ablation in T1 renal cell carcinoma: Initial results in clinical routine," *Biomed. Res. Int.*, vol. 2021, May 2021, Art. no. 5537192, doi: 10.1155/2021/5537192.

[48] T. L. De Jong, N. J. van de Berg, L. Tas, A. Moelker, J. Dankelman, and J. J. van den Dobbelsteen, "Needle placement errors: Do we need steerable needles in interventional radiology?" *Med. Devices Evid. Res.*, vol. 11, pp. 259–265, Aug. 2018, doi: 10.2147/MDER.S160444.

[49] E. Ben-David, M. Shochat, I. Roth, I. Nissenbaum, J. Sosna, and S. N. Goldberg, "Evaluation of a CT-guided robotic system for precise percutaneous needle insertion," *J. Vascular Interventional Radiol.*, vol. 29, no. 10, pp. 1440–1446, Oct. 2018, doi: 10.1016/J.JVIR.2018.01.002.

[50] M. Ahmed et al., "Image-guided tumor ablation: Standardization of terminology and reporting Criteria-A 10-year update," *Radiology*, vol. 273, no. 1, pp. 241–260, Jun. 2014, doi: 10.1148/radiol.14132958.

[51] G. Laimer et al., "Volumetric assessment of the periablational safety margin after thermal ablation of colorectal liver metastases," *Eur. Radiol.*, vol. 31, no. 9, pp. 6489–6499, 2021, doi: 10.1007/s00330-020-07579-x.

[52] A. Seitel et al., "Computer-assisted trajectory planning for percutaneous needle insertions," *Med. Phys.*, vol. 38, no. 6Part1, pp. 3246–3259, 2011, doi: 10.1118/1.3590374.

[53] J. Schaible et al., "Safety margin assessment after microwave ablation of liver tumors: Inter- and intrareader variability," *Radiol. Oncol.*, vol. 54, no. 1, pp. 57–61, Feb. 2020, doi: 10.2478/RAON-2020-0004.

[54] X. Buy, H. Lang, J. Garnon, E. Sauleau, C. Roy, and A. Gangi, "Percutaneous renal cryoablation: Prospective experience treating 120 consecutive tumors," *Am. J. Roentgenol.*, vol. 201, no. 6, pp. 1353–1361, Dec. 2013, doi: 10.2214/AJR.13.11084.

[55] G. Laimer, P. Schullian, R. Bale, J. M. R. Bélanger, and J. R. J. Paré, "Stereotactic thermal ablation of liver tumors: 3D planning, multiple needle approach, and intraprocedural image fusion are the key to success—A narrative review," *Biology*, vol. 10, no. 7, 2021, Art. no. 644, doi: 10.3390/BIOLOGY10070644.

[56] P. De Marini et al., "Safety and oncologic efficacy of percutaneous MRI-guided cryoablation of intraparenchymal renal cancers," *Diagnostic Interventional Imag.*, vol. 102, no. 9, pp. 531–538, Sep. 2021, doi: 10.1016/J.DIII.2021.04.002.

[57] J. P. Kühn et al., "Magnetic resonance-guided upper abdominal biopsies in a high -field wide-bore 3-T MRI system: Feasibility, handling, and needle artefacts," *Eur. Radiol.*, vol. 20, no. 10, pp. 2414–2421, 2010, doi: 10.1007/s00330-010-1809-4.

[58] S. Singh, F. Torrealdea, and S. Bandula, "MR imaging–guided intervention: Evaluation of MR conditional biopsy and ablation needle tip artifacts at 3T using a balanced fast field echo sequence," *J. Vascular Interventional Radiol.*, vol. 32, no. 7, pp. 1068–1074.e1, 2021, doi: 10.1016/j.jvir.2021.03.536.

[59] T. Penzkofer, N. Peykan, K. Schmidt, G. Krombach, and C. K. Kuhl, "How MRI compatible is 'mRI compatible'? A systematic comparison of artifacts caused by biopsy needles at 3.0 and 1.5 T," *Cardiovascular Interventional Radiol.*, vol. 36, no. 6, pp. 1646–1657, 2013, doi: 10.1007/s00270-013-0616-0.

[60] B. Maurin et al., "In vivo study of forces during needle insertions," in *Proc. Sci. Workshop Med. Robot., Navigation Visualization, RheinAhrCampus*, Remagen, Germany, 2004, pp. 415–422, doi: 10.1142/9789812702678_0056.

[61] L. H. Poniatowski, S. S. Somani, D. Veneziano, S. McAdams, and R. M. Sweet, "Characterizing and simulating needle insertion forces for percutaneous renal access," *J. Endourol.*, vol. 30, no. 10, pp. 1049–1055, 2016, doi: 10.1089/end.2016.0342.

[62] K. W. Ng, J. Q. Goh, S. L. Foo, P. H. Ting, and T. K. Lee, "Needle insertion forces studies for optimal surgical modeling," *Int. J. Biosci. Biochem. Bioinf.*, vol. 3, no. 3, pp. 187–191, 2013, doi: 10.7763/ijbbb.2013.v3.193.

[63] A. Majewicz et al., "Behavior of tip-steerable needles in ex vivo and in vivo tissue," *IEEE Trans. Biomed. Eng.*, vol. 59, no. 10, pp. 2705–2715, 2012, doi: 10.1109/TBME.2012.2204749.

[64] D. J. Van Gerwen, J. Dankelman, and J. J. Van Den Dobbelsteen, "Measurement and stochastic modeling of kidney puncture forces," *Ann. Biomed. Eng.*, vol. 42, no. 3, pp. 685–695, 2014, doi: 10.1007/s10439-013-0924-1.

[65] T. Yamanaka et al., "CT-guided percutaneous cryoablation in renal cell carcinoma: Factors affecting local tumor control," *J. Vascular Interventional Radiol.*, vol. 26, no. 8, pp. 1147–1153, 2015, doi: 10.1016/j.jvir.2015.04.031.

[66] T. L. de Jong, S. J. C. Klink, A. Moelker, J. Dankelman, and J. J. van den Dobbelsteen, "Needle deflection in thermal ablation procedures of liver tumors: A CT image analysis," in *Proc. SPIE*, Mar. 2018, pp. 8, doi: 10.1117/12.2292884.

[67] E. Franco and M. Ristic, "Design and control of needle positioner for MRI-guided laser ablation of the liver," in *Proc. IEEE/ASME 10th Int. Conf. Mechatron. Embedded Syst. Appl. (MESA)*, Senigallia, Italy, Oct. 2014, pp. 1–6, doi: 10.1109/MESA.2014.6935546.

[68] T. de Baère, C. Roux, F. Deschamps, L. Tselikas, and B. Guiu, "Evaluation of a new CT-guided robotic system for percutaneous needle insertion for thermal ablation of liver tumors: A prospective pilot study," *Cardiovascular Interventional Radiol.*, vol. 45, no. 11, pp. 1701–1709, 2022, doi: 10.1007/s00270-022-03267-z.

[69] T. de Baere et al., "Robotic assistance for percutaneous needle insertion in the kidney: Preclinical proof on a swine animal model," *Eur. Radiol. Exp.*, vol. 6, no. 1, pp. 1701–1709, 2022, doi: 10.1186/s41747-022-00265-1.

[70] A. Adnan and R. A. Sheth, "Image-guided percutaneous biopsy of the liver," *Techn. Vascular Interventional Radiol.*, vol. 24, no. 4, 2021, Art. no. 100773, doi: 10.1016/j.tvir.2021.100773.

[71] N. I. Sainani, R. S. Arellano, P. B. Shyn, D. A. Gervais, P. R. Mueller, and S. G. Silverman, "The challenging image-guided abdominal mass biopsy: Established and emerging techniques 'if you can see it, you can biopsy it," *Abdominal Imag.*, vol. 38, no. 4, pp. 672–696, 2013, doi: 10.1007/s00261-013-9980-0.

[72] N. A. Patel et al., "System integration and preliminary clinical evaluation of a robotic system for MRI-guided transperineal prostate biopsy," *J. Med. Robot. Res.*, vol. 04, no. 02, Jun. 2019, Art. no. 1950001, doi: 10.1142/S2424905X6.

[73] I. Seimenis, N. V. Tsekos, C. Keroglou, E. Eracleous, C. Pitris, and E. G. Christoforou, "An approach for preoperative planning and performance of MR-guided interventions demonstrated with a manual manipulator in a 1.5T MRI scanner," *Cardiovascular Interventional Radiol.*, vol. 35, no. 2, pp. 359–367, Apr. 2012, doi: 10.1007/s00270-011-0147-5.

[74] I. Bricault et al., "Light puncture robot for CT and MRI interventions," *IEEE Eng. Med. Biol. Mag.*, vol. 27, no. 3, pp. 42–50, May/Jun. 2008, doi: 10.1109/EMB.2007.910262,

[75] K. H. Wong, J. W. VanMeter, S. T. Fricke, C. R. Maurer, and K. Cleary, "MRI for modeling of liver and skin respiratory motion," *Int. Congr. Ser.*, vol. 1268, no. C, pp. 747–752, 2004, doi: 10.1016/j.ics.2004.03.215.

[76] N. Hata, F. Ohara, R. Hashimoto, M. Hashizume, and T. Dohi, "Needle guiding robot with five-bar linkage for MR-guided thermotherapy of liver tumor," in *Proc. Int. Conf. Med. Image Comput. Comput.-Assisted Intervention*, Berlin, Germany: Springer-Verlag, 2004, pp. 161–168, doi: 10.1007/978-3-540-30136-3_21.

[77] K. Masamune, F. Ohara, K. Matsumiya, H. Liao, M. Hashizume, and T. Dohi, "MRI compatible robot for needle placement therapy with accurate registration," in *Proc. World Congr. Med. Phys. Biomed. Eng.*, vol. 14, Berlin, Germany: Springer-Verlag, 2007, pp. 3056–3059, doi: 10.1007/978-3-540-36841-0_774.

[78] I. Sato, R. Nakamura, and K. Masamune, "MRI compatible manipulator with MRI-guided needle insertion support system," in *Proc. Int. Symp. Micro-NanoMechatron. Human Sci.*, Nagoya, Japan, 2010, pp. 77–82, doi: 10.1109/MHS.2010.5669573.

[79] E. Franco, M. Aurisicchio, and M. Ristic, "Design and control of 3-DOF needle positioner for MRI-guided laser ablation of liver tumours," *J. Biomechatron. Biomed. Robot.*, vol. 3, no. 3, pp. 10–12, 2014.

[80] E. Franco, M. Ristic, M. Rea, and W. M. W. Gedroyc, "Robot-assistant for MRI-guided liver ablation: A pilot study," *Med. Phys.*, vol. 43, no. 10, pp. 5347–5356, Oct. 2016, doi: 10.1118/1.4961986.

[81] G. Bouliane-Blais and J.-S. Plante, "Design of a soft multi-degree of freedom tool positioner with variable stiffness integrating molded air muscles actuation, granular jamming and dielectric elastomer sensing," in *Proc. Int. Design Eng. Techn. Conf. Comput. Inf. Eng. Conf.*, New York, NY, USA: American Society of Mechanical Engineers Digital Collection, Jan. 2015, doi: 10.1115/detc2015-47877.

[82] J. Ghelfi et al., "Evaluation of the needle positioning accuracy of a light puncture robot under MRI guidance: Results of a clinical trial on healthy volunteers," *Cardiovascular Interventional Radiol.*, vol. 41, no. 9, pp. 1428–1435, Sep. 2018, doi: 10.1007/S00270-018-2001-5/TABLES/2.

[83] A. Reichert, M. Bock, M. Vogele, and A. J. Krafft, "GantryMate: A modular MR-compatible assistance system for MR-guided needle interventions," *Tomography*, vol. 5, no. 2, pp. 266–273, Jun. 2019, doi: 10.18383/J.TOM.2019.00007.

[84] S. Morikawa et al., "Preliminary clinical experiences of a motorized manipulator for magnetic resonance image-guided microwave coagulation therapy of liver tumors," *Am. J. Surg.*, vol. 198, no. 3, pp. 340–347, Sep. 2009, doi: 10.1016/j.amjsurg.2009.02.006.

[85] N. Hata, J. Tokuda, S. Hurwitz, and S. Morikawa, "MRI-compatible manipulator with remote-center-of-motion control," *J. Magn. Reson. Imag.*, vol. 27, no. 5, pp. 1130–1138, May 2008, doi: 10.1002/jmri.21314.

[86] N. Hata, R. Hashimoto, J. Tokuda, and S. Morikawa, "Needle guiding robot for MR-guided microwave thermotherapy of liver tumor using motorized remote-center-of-motion constraint," in *Proc. IEEE Int. Conf. Robot. Automat.*, Barcelona, Spain, 2005, pp. 1652–1656, doi: 10.1109/ROBOT.2005.1570350.

[87] A. Bruyas, F. Geiskopf, and P. Renaud, "Toward unibody robotic structures with integrated functions using multimaterial additive manufacturing: Case study of an MRI-compatible interventional device," in *Proc. IEEE/RSJ Int. Conf. Intell. Robot. Syst. (IROS)*, Hamburg, Germany, Dec. 2015, pp. 1744–1750, doi: 10.1109/IROS.2015.7353603.

[88] S. Frishman, R. D. Ings, V. Sheth, B. L. Daniel, and M. R. Cutkosky, "Extending reach inside the MRI bore: A 7-DOF, low-friction, hydrostatic teleoperator," *IEEE Trans. Med. Robot. Bionics*, vol. 3, no. 3, pp. 701–713, Aug. 2021, doi: 10.1109/TMRB.2021.3097123.

[89] N. V. Tsekos, A. Özcan, and E. Christoforou, "A prototype manipulator for magnetic resonance-guided interventions inside standard cylindrical magnetic resonance imaging scanners," *J. Biomech. Eng.*, vol. 127, no. 6, pp. 972–980, Nov. 2005, doi: 10.1115/1.2049339.

[90] E. G. Christoforou, N. Y. Tsekos, and A. Özcan, "Design and testing of a robotic system for MR image-guided interventions," *J. Intell. Robot. Syst. Theory Appl.*, vol. 47, no. 2, pp. 175–196, Sep. 2006, doi: 10.1007/s10846-006-9082-0.

[91] E. Christoforou, E. Akbudak, A. Ozcan, M. Karanikolas, and N. V. Tsekos, "Performance of interventions with manipulator-driven real-time MR guidance: Implementation and initial in vitro tests," *Magn. Reson. Imag.*, vol. 25, no. 1, pp. 69–77, Jan. 2007, doi: 10.1016/J.MRI.2006.08.016.

[92] A. Öcan and N. Tsekos, "The interconnection of MRI scanner and MR-compatible robotic device: Synergistic graphical user interface to form a mechatronic system," *IEEE/ASME Trans. Mechatron.*, vol. 13, no. 3, pp. 362–369, Jun. 2008, doi: 10.1109/TMECH.2008.924120.

[93] E. G. Christoforou, I. Seimenis, E. Andreou, E. Eracleous, and N. V. Tsekos, "A novel, general-purpose, MR-compatible, manually actuated robotic manipulation system for minimally invasive interventions under direct MRI guidance," *Int. J. Med. Robot. Comput. Assisted Surg.*, vol. 10, no. 1, pp. 22–34, Mar. 2014, doi: 10.1002/rcs.1504.

[94] E. Franco and M. Ristic, "MRI-compatible needle positioner for laser ablation of the liver: Preliminary evaluation in a 3T MRI scanner," in *Proc. Hamlyn Symp. Med. Robot.*, 2014, p. 73.

[95] B. Gherman et al., "Risk assessment-oriented design of a needle insertion robotic system for non-resectable liver Tumors," *Healthcare*, vol. 10, no. 2, 2022, Art. no. 389, doi: 10.3390/HEALTHCARE10020389.

[96] S. Frishman, A. Kight, I. Pirozzi, M. C. Coffey, B. L. Daniel, and M. R. Cutkosky, "Enabling in-bore MRI-guided biopsies with force feedback," *IEEE Trans. Haptics*, vol. 13, no. 1, pp. 159–166, Jan. 2020, doi: 10.1109/TOH.2020.2967375.

[97] N. Burkhard et al., "A rolling-diaphragm hydrostatic transmission for remote MR-guided needle insertion," in *Proc. IEEE Int. Conf. Robot. Automat.*, Institute of Electrical and Electronics Engineers Inc., July 2017, pp. 1148–1153, doi: 10.1109/ICRA.2017.7989137.

[98] Z. Guo et al., "Compact design of a hydraulic driving robot for intraoperative MRI-guided bilateral stereotactic neurosurgery," *IEEE Robot. Autom. Lett.*, vol. 3, no. 3, pp. 2515–2522, 2018, doi: 10.1109/LRA.2018.2814637.

[99] E. Taillant, J. C. Avila-Vilchis, C. Allegrini, I. Bricault, and P. Cinquin, "CT and MR compatible light puncture robot: Architectural design and first experiments," in *Proc. Int. Conf. Med. Image Comput. Comput.-Assisted Intervention*, Heidelberg, Germany: Springer-Verlag, 2004, pp. 145–152, doi: 10.1007/978-3-540-30136-3_19.

[100] N. Zemiti, I. Bricault, C. Fouard, B. Sanchez, and P. Cinquin, "LPR: A CT and MR-compatible puncture robot to enhance accuracy and safety of image-guided interventions," *IEEE/ASME Trans. Mechatron.*, vol. 13, no. 3, pp. 306–315, Jun. 2008, doi: 10.1109/TMECH.2008.924045.

[101] J. Tokuda et al., "Motion compensation for MRI-compatible patient-mounted needle guide device: Estimation of targeting accuracy in MRI-guided kidney cryoablations," *Phys. Med. Biol.*, vol. 63, no. 8, Apr. 2018, Art. no. 085010, doi: 10.1088/1361-6560/aab736.

[102] C. Watkins, T. Kato, and N. Hata, "Disposable patient-mounted geared robot for image-guided needle insertion," in *Proc. SPIE*, Mar. 2016, p. 97860S, doi: 10.1117/12.2216779.

[103] N. Shono et al., "Simulated accuracy assessment of small footprint body-mounted probe alignment device for MRI-guided cryotherapy of abdominal lesions," *Med. Phys.*, vol. 47, no. 6, pp. 2337–2349, Jun. 2020, doi: 10.1002/mp.14116.

[104] N. Hata et al., "Body-mounted robotic instrument guide for image-guided cryotherapy of renal cancer," *Med. Phys.*, vol. 43, no. 2, pp. 843–853, Feb. 2016, doi: 10.1118/1.4939875.

[105] F. Y. Wu et al., "An MRI coil-mounted multi-probe robotic positioner for cryoablation," in *Proc. ASME Design Eng. Tech. Conf.*, New York, NY, USA: American Society of Mechanical Engineers Digital Collection, Feb. 2013, doi: 10.1115/DETC2013-13132.

[106] Z. He et al., "Design of a percutaneous MRI-guided needle robot with soft fluid-driven actuator," *IEEE Robot. Automat. Lett.*, vol. 5, no. 2, pp. 2100–2107, Apr. 2020, doi: 10.1109/LRA.2020.2969929.

[107] C. C. Roberts, W. B. Morrison, D. M. Deely, A. C. Zoga, G. Koulouris, and C. S. Winalski, "Use of a novel percutaneous biopsy localization device: Initial musculoskeletal experience," *Skeletal Radiol.*, vol. 36, no. 1, pp. 53–57, Jan. 2007, doi: 10.1007/S00256-006-0182-5/FIGURES/3.

[108] A. Bruyas, F. Geiskopf, and P. Renaud, "Design and modeling of a large amplitude compliant revolute joint: The helical shape compliant joint," *J. Mech. Des.*, vol. 137, no. 8, Aug. 2015, Art. no. 085003, doi: 10.1115/1.4030650.

[109] A. Pfeil, L. Barbe, B. Wach, R. L. Cazzato, A. Gangi, and P. Renaud, "Observations and experiments for the definition of a new robotic device dedicated to CT, CBCT and MRI-guided percutaneous procedures," in *Proc. Annu. Int. Conf. IEEE Eng. Med. Biol. Soc. (EMBC)*, Honolulu, HI, USA, Oct. 2018, pp. 1708–1712, doi: 10.1109/EMBC.2018.8512682.

[110] M. Musa, S. Sengupta, and Y. Chen, "Design of a 6 DoF parallel robot for MRI-guided interventions," in *Proc. Int. Symp. Med. Robot. (ISMR)*, Atlanta, GA, USA, 2021, pp. 1–7, doi: 10.1109/ISMR48346.2021.9661513.

[111] E. Franco and M. Ristic, "Adaptive control of a master-slave system for teleoperated needle insertion under MRI-guidance," in *Proc. 23rd Mediterranean Conf. Control Automat. (MED)*, Torremolinos, Spain, Jul. 2015, pp. 61–67, doi: 10.1109/MED.2015.7158730.

[112] E. Franco, M. Rea, W. Gedroyc, and M. Ristic, "Control of a master–slave pneumatic system for teleoperated needle insertion in MRI," *IEEE/ASME Trans. Mechatron.*, vol. 21, no. 5, pp. 2595–2600, Oct. 2016, doi: 10.1109/TMECH.2016.2577608.

[113] A. Pfeil et al., "A 3D-printed needle driver based on auxetic structure and inchworm kinematics," in *Proc. ASME Int. Design Eng. Tech. Conf. Comput. Inf. Eng. Conf.*, New York, NY, USA: American Society of Mechanical Engineers Digital Collection, Nov. 2018, doi: 10.1115/detc2018-85371.

[114] K. El Bannan, B. A. Chronik, and S. P. Salisbury, "Development of an MRI-compatible, compact, rotary-linear piezoworm actuator," *J. Med. Devices, Trans. ASME*, vol. 9, no. 1, Mar. 2015, Art. no. 014501, doi: 10.1115/1.4028943/376738.

[115] A. Vaccarella, E. De Momi, A. Enquobahrie, and G. Ferrigno, "Unscented Kalman filter based sensor fusion for robust optical and electromagnetic tracking in surgical navigation," *IEEE Trans. Instrum. Meas.*, vol. 62, no. 7, pp. 2067–2081, Jul. 2013, doi: 10.1109/TIM.2013.2248304.

[116] J. H. Bae and S. H. Chang, "PVDF-based ferroelectric polymers and dielectric elastomers for sensor and actuator applications: A review," *Functional Composites Struct.*, vol. 1, no. 1, Mar. 2019, Art. no. 012003, doi: 10.1088/2631-6331/AB0F48.

[117] V. P. B. Grover, J. M. Tognarelli, M. M. E. Crossey, I. J. Cox, S. D. Taylor-Robinson, and M. J. W. McPhail, "Magnetic resonance imaging: Principles and techniques: Lessons for clinicians," *J. Clin. Exp. Hepatol.*, vol. 5, no. 3, pp. 246–255, Sep. 2015, doi: 10.1016/J.JCEH.2015.08.001.

[118] A. Reichert, M. Bock, S. Reiss, C. G. Overduin, J. J. Fütterer, and A. J. Krafft, "Simultaneous slice excitation for accelerated passive marker tracking via phase-only cross correlation (POCC) in MR-guided needle interventions," *MAGMA*, vol. 31, no. 6, pp. 781–788, Dec. 2018, doi: 10.1007/S10334-018-0701-0.

[119] É. Dorileo, N. Zemiti, S. Krut, and P. Poignet, "CT/MR-compatible physical human-robotized needle interactions: From modeling to percutaneous steering," *Mechatronics*, vol. 85, Aug. 2022, Art. no. 102840, doi: 10.1016/J.MECHATRONICS.2022.102840.

[120] W. Shang, H. Su, G. Li, and G. S. Fischer, "Teleoperation system with hybrid pneumatic-piezoelectric actuation for MRI-guided needle insertion with haptic feedback," in *Proc. IEEE/RSJ Int. Conf. Intell. Robot. Syst.*, Tokyo, Japan, 2013, pp. 4092–4098, doi: 10.1109/IROS.2013.6696942.

[121] E. Franco, "Combined adaptive and predictive control for a teleoperation system with force disturbance and input delay," *Frontiers Robot. AI*, vol. 3, Aug. 2016, Art. no. 48, doi: 10.3389/FROBT.2016.00048/BIBTEX.

[122] M. R. Van Den Bosch et al., "MRI-guided robotic system for transperineal prostate interventions: Proof of principle," *Phys. Med. Biol.*, vol. 55, no. 5, pp. N133–N140, Feb. 2010, doi: 10.1088/0031-9155/55/5/N02.

[123] S. E. Song et al., "Preliminary evaluation of a MRI-compatible modular robotic system for MRI-guided prostate interventions," in *Proc. 3rd IEEE RAS EMBS Int. Conf. Biomed. Robot. Biomechatron.*, Tokyo, Japan, 2010, pp. 796–801, doi: 10.1109/BIOROB.2010.5626987.

[124] P. Moreira et al., "The MIRIAM robot: A novel robotic system for MR-guided needle insertion in the prostate," *J. Med. Robot. Res.*, vol. 02, no. 04, Dec. 2017, Art. no. 1750006, doi: 10.1142/S2424905X17500064.

[125] V. Groenhuis, F. J. Siepel, J. Veltman, J. K. van Zandwijk, and S. Stramigioli, "Stormram 4: An MR safe robotic system for breast biopsy," *Ann. Biomed. Eng.*, vol. 46, no. 10, pp. 1686–1696, Oct. 2018, doi: 10.1007/s10439-018-2051-5.

[126] T. Zhang, D. Navarro-Alarcon, K. W. Ng, M. K. Chow, Y. H. Liu, and H. L. Chung, "A novel palm-shape breast deformation robot for MRI-guided biopsy," in *Proc. IEEE Int. Conf. Robot. Biomimetics (ROBIO)*, Qingdao, China, 2016, pp. 527–532, doi: 10.1109/ROBIO.2016.7866376.

[127] A. Melzer et al., "INNOMOTION for percutaneous image-guided interventions," *IEEE Eng. Med. Biol. Mag.*, vol. 27, no. 3, pp. 66–73, May 2008, doi: 10.1109/EMB.2007.910274.

[128] M. Li, D. Mazilu, B. J. Wood, K. A. Horvath, and A. Kapoor, "A robotic assistant system for cardiac interventions under MRI guidance," in *Proc. Med. Imag., Visualization, Image-Guided Procedures, Model.*, SPIE, Feb. 2010, pp. 920–929, doi: 10.1117/12.844458.

[129] M. Li, A. Kapoor, D. Mazilu, and K. A. Horvath, "Pneumatic actuated robotic assistant system for aortic valve replacement under MRI guidance," *IEEE Trans. Biomed. Eng.*, vol. 58, no. 2, pp. 443–451, Feb. 2011, doi: 10.1109/TBME.2010.2089983.

[130] E. Hempel et al., "An MRI-compatible surgical robot for precise radiological interventions," *Comput. Aided Surg.*, vol. 8, no. 4, pp. 180–191, 2003, doi: 10.3109/10929080309146052.

[131] R. Monfaredi et al., "A prototype body-mounted MRI-compatible robot for needle guidance in shoulder arthrography," in *Proc. IEEE. RAS. EMBS. Int. Conf. Biomed. Robot. Biomechatronics*, Sep. 2014, vol. 2014, p. 40, doi: 10.1109/BIOROB.2014.6913749.

[132] R. Monfaredi et al., "Development of a shoulder-mounted robot for MRI-guided needle placement: Phantom study," *Int. J. Comput. Assisted Radiol. Surgery*, vol. 13, no. 11, pp. 1829–1841, Nov. 2018, doi: 10.1007/S11548-018-1839-Y/TABLES/4.

[133] N. A. Patel, E. Azimi, R. Monfaredi, K. Sharma, K. Cleary, and I. Iordachita, "Robotic system for MRI-guided shoulder arthrography: Accuracy evaluation," in *Proc. Int. Symp. Med. Robot. (ISMR)*, Piscataway, NJ, USA: Institute of Electrical and Electronics Engineers, Apr. 2018, pp. 1–6, doi: 10.1109/ISMR.2018.8333299.

[134] G. H. Kim et al., "Shoulder-mounted Robot for MRI-Guided Arthrography: Clinically Optimized System," in *Proc. Annu. Int. Conf. IEEE Eng. Med. Biol. Soc. (EMBS)*, Jul. 2019, pp. 1977–1980, doi: 10.1109/EMBC.2019.8856630.

[135] N. Patel et al., "Body-mounted robotic system for MRI-guided shoulder arthrography: cadaver and clinical workflow studies," *Frontiers Robot. AI*, vol. 8, May 2021, Art. no. 125, doi: 10.3389/FROBT.2021.667121/BIBTEX.

[136] N. Patel, J. Yan, R. Monfaredi, K. Sharma, K. Cleary, and I. Iordachita, "Preclinical evaluation of an integrated robotic system for magnetic resonance imaging guided shoulder arthrography," *J. Med. Imag.*, vol. 6, no. 2, May 2019, p. 1, doi: 10.1117/1.JMI.6.2.025006.

[137] N. A. Patel, J. Yan, D. Levi, R. Monfaredi, K. Cleary, and I. Iordachita, "Body-mounted robot for image-guided percutaneous interventions: Mechanical design and preliminary accuracy evaluation," in *Proc. IEEE Int. Conf. Intell. Robots Syst. (IROS)*, Dec. 2018, pp. 1443–1448, doi: 10.1109/IROS.2018.8593807.

[138] J. Yan, N. Patel, G. L. Di Wu, K. Cleary, and I. Iordachita, "Body-mounted MRI-conditional parallel robot for percutaneous interventions structural improvement, calibration, and accuracy analysis," in *Proc. IEEE Annu. Int. Conf. IEEE Eng. Med. Biol. Soc. (EMBC)*, Jul. 2019, pp. 1990–1993, doi: 10.1109/EMBC.2019.8857667.

[139] J. S. Kim, D. Levi, R. Monfaredi, K. Cleary, and I. Iordachita, "A new 4-DOF parallel robot for MRI-guided percutaneous interventions: Kinematic analysis," in *Proc. Annu. Int. Conf. IEEE Eng. Med. Biol. Soc. (EMBS)*, Piscataway, NJ, USA: Institute of Electrical and Electronics Engineers, Sep. 2017, pp. 4251–4255, doi: 10.1109/EMBC.2017.8037795.

[140] D. Wu et al., "Remotely actuated needle driving device for MRI-guided percutaneous interventions," in *Proc. Int. Symp. Med. Robot. (ISMR)*, May 2019, pp. 1–7, doi: 10.1109/ISMR.2019.8710176.

[141] G. Li et al., "Body-mounted robotics for interventional MRI procedures," *IEEE Trans. Med. Robot. Bionics*, vol. 2, no. 4, pp. 557–560, Nov. 2020, doi: 10.1109/TMRB.2020.3030532.

[142] Y. Wang, G. Li, K. W. Kwok, K. Cleary, R. H. Taylor, and I. Iordachita, "Towards safe in situ needle manipulation for robot assisted lumbar injection in interventional MRI," in *Proc. IEEE Int. Conf. Intell. Robots Syst.*, Piscataway, NJ, USA: Institute of Electrical and Electronics Engineers, 2021, pp. 1835–1842, doi: 10.1109/IROS51168.2021.9636220.

[143] G. Li et al., "Fully actuated body-mounted robotic system for MRI-guided lower back pain injections: Initial phantom and cadaver studies," *IEEE Robot. Autom. Lett.*, vol. 5, no. 4, pp. 5245–5251, Oct. 2020, doi: 10.1109/LRA.2020.3007459.

[144] G. Li, N. A. Patel, A. Melzer, K. Sharma, I. Iordachita, and K. Cleary, "MRI-guided lumbar spinal injections with body-mounted robotic system: Cadaver studies," *Minimally Invasive Ther. Allied Technol.*, vol. 31, no. 2, pp. 297–305, 2022, doi: 10.1080/13645706.2020.1799017.

[145] G. Li et al., "Body-mounted robotic assistant for MRI-guided low back pain injection," *Int. J. Comput. Assisted Radiol. Surgery*, vol. 15, no. 2, pp. 321–331, Feb. 2020, doi: 10.1007/S11548-019-02080-3/FIGURES/10.

[146] M. Oura, Y. Kobayashi, J. Okamoto, and M. G. Fujie, "Development of MRI compatible versatile manipulator for minimally invasive surgery -Prototype of positioning manipulator," in *Proc. 1st IEEE/RAS-EMBS Int. Conf. Biomed. Robot. Biomechatronics*, 2006, vol. 2006, pp. 176–181, doi: 10.1109/BIOROB.2006.1639080.

[147] B. Zhao, Y. Fu, Y. Yang, P. Zhang, and Y. Hu, "Design and control of a MRI-compatible pneumatic needle puncture robot," *Comput. Assisted Surgery*, vol. 24, no. sup2, pp. 87–93, Oct. 2019, doi: 10.1080/24699322.2019.1649067.

[148] X. Xiang, "A localization framework under non-rigid deformation for robotic surgery," in *Proc. Adv. Vis. Comput.*, 2011, vol. 6938 LNCS, no. PART 1, pp. 11–22, doi: 10.1007/978-3-642-24028-7_2/COVER/.

[149] Q. Boehler, M. Vedrines, S. Abdelaziz, P. Poignet, and P. Renaud, "Design and evaluation of a novel variable stiffness spherical joint with application to MR-compatible robot design," in *Proc. - IEEE Int. Conf. Robot. Autom.*, vol. 2016-June, pp. 661–667, Jun. 2016, doi: 10.1109/ICRA.2016.7487192.

[150] K. Masamune et al., "Development of an MRI-compatible needle insertion manipulator for stereotactic neurosurgery," *Comput. Aided Surgery*, vol. 1, no. 4, pp. 242–248, 1995, doi: 10.3109/10929089509106330.

[151] K. Masamune, M. Sonderegger, M. Suzuki, T. Dohi, H. Iseki, and K. Takakura, "Robots for stereotactic neurosurgery," *Adv. Robot.*, vol. 10, no. 4, pp. 391–401, 1995, doi: 10.1163/156855396X00057.

[152] G. Li, N. A. Patel, E. C. Burdette, J. G. Pilitsis, H. Su, and G. S. Fischer, "A fully actuated robotic assistant for MRI-guided precision conformal ablation of brain tumors," *IEEE/ASME Trans. Mechatronics*, vol. 26, no. 1, pp. 255–266, Feb. 2021, doi: 10.1109/TMECH.2020.3012903.

[153] N. A. Patel et al., "An integrated robotic system for MRI-guided neuroablation: Preclinical evaluation," *IEEE Trans. Biomed. Eng.*, vol. 67, no. 10, pp. 2990–2999, Oct. 2020, doi: 10.1109/TBME.2020.2974583.

[154] Y. Qiu, L. Wu, F. Huang, Z. Huang, Q. Yan, and J. Guo, "MRI-compatible hydraulic drive needle insertion robot," in *Proc. 6th IEEE Int. Conf. Adv. Robot. Mechatronics (ICARM)*, Jul. 2021, pp. 86–92, doi: 10.1109/ICARM52023.2021.9536120.

[155] K. Cleary et al., "Robotically assisted long bone biopsy under MRI imaging: Workflow and preclinical study," *Acad. Radiol.*, vol. 25, no. 1, pp. 74–81, Jan. 2018, doi: 10.1016/j.acra.2017.08.008.

[156] S. Lim et al., "Robotically assisted long bone biopsy under MRI: Cadaver study results," *Int. J. Comput. Assisted Radiol. Surgery*, vol. 14, no. 1, pp. 147–156, Jan. 2019, doi: 10.1007/s11548-018-1889-1.

[157] D. Stoianovici et al., "Multi-imager compatible, MR safe, remote center of motion needle-guide robot," *IEEE Trans. Biomed. Eng.*, vol. 65, no. 1, pp. 165–177, Jan. 2018, doi: 10.1109/TBME.2017.2697766.

[158] Z. Hong, C. Yun, and L. Zhao, "A MRI-guided robot for neurosurgery: Design and control," in *Proc. IEEE Int. Conf. Inf. Autom. (ICIA)*, 2008, pp. 759–764, doi: 10.1109/ICINFA.2008.4608100.

[159] Z. Hong, C. Yun, L. Zhao, and Y. Wang, "A MRI-guided robot for neurosurgery: Optimization, registration and tracking," in *Proc. Chin. Control Decis. Conf. (CCDC)*, 2008, pp. 2222–2227, doi: 10.1109/CCDC.2008.4597718.

[160] X. Xiao et al., "Portable body-attached positioning mechanism toward robotic needle intervention," *IEEE/ASME Trans. Mechatronics*, vol. 25, no. 2, pp. 1105–1116, Apr. 2020, doi: 10.1109/TMECH.2020.2974760.

[161] A. Salimi, A. Ramezanifar, J. Mohammadpour, K. Grigoriadis, and N. V. Tsekos, "ROBOCATH: A patient-mounted parallel robot to position and orient surgical catheters," in *Proc. ASME 5th Annu. Dyn. Syst. Control Conf. Joint JSME 11th Motion Vibration Conf., (DSCC)*, American Society of Mechanical Engineers Digital Collection, Sep. 2012, pp. 471–480, doi: 10.1115/DSCC2012-MOVIC2012-8846.

[162] Y. Kobayashi, J. Okamoto, and M. G. Fujie, "Physical properties of the liver and the development of an intelligent manipulator for needle insertion," in *Proc. - IEEE Int. Conf. Robot. Autom.*, 2005, vol. 2005, pp. 1632–1639, doi: 10.1109/ROBOT.2005.1570347.

[163] T. Cui, Y. Wang, X. Duan, and X. Ma, "Control strategy and experiments for robot assisted craniomaxillofacial surgery system," *Math. Problem Eng*, vol. 2019, Mar. 2019, Art. no. 4853046, doi: 10.1155/2019/4853046.

[164] X. Duan, L. Gao, Y. Wang, J. Li, H. Li, and Y. Guo, "Modelling and experiment based on a navigation system for a cranio-maxillofacial surgical robot," *J. Healthcare Eng.*, vol. 2018, 2018, Art. no. 4670852, doi: 10.1155/2018/4670852.

[165] J. R. J. Realpe, G. Aiche, S. Abdelaziz, and P. Poignet, "Asynchronous and decoupled control of the position and the stiffness of a spatial RCM tensegrity mechanism for needle manipulation," in *Proc. IEEE Int. Conf. Robot. Autom.*, May 2020, pp. 3882–3888, doi: 10.1109/ICRA40945.2020.9197507.

[166] J. Li and Q. Jiang, "Optimal design and experiment of cable-driven puncturing surgery robot for soft needle," *J. Med. Device*, vol. 17, no. 2, Jun. 2023, Art. no. 021008, doi: 10.1115/1.4056865.

[167] D. Ma, "Research progress and development direction of structural optimization and modeling of traveling wave rotating ultrasonic motor," in *Proc. 4th World Conf. Mech. Eng. Intell. Manuf. (WCMEIM)*, 2021, pp. 442–447, doi: 10.1109/WCMEIM54377.2021.00096.

[168] D. Stoianovici, A. Patriciu, D. Petrisor, D. Mazilu, and L. Kavoussi, "A new type of motor: Pneumatic step motor," *IEEE/ASME Trans. Mechatronics*, vol. 12, no. 1, pp. 98–106, Feb. 2007, doi: 10.1109/TMECH.2006.886258.

[169] V. Groenhuis and S. Stramigioli, "Rapid prototyping high-performance MR safe pneumatic stepper motors," *IEEE/ASME Trans. Mechatronics*, vol. 23, no. 4, pp. 1843–1853, Aug. 2018, doi: 10.1109/TMECH.2018.2840682.

[170] M. E. M. K. Abdelaziz, V. Groenhuis, J. Veltman, F. Siepel, and S. Stramigioli, "Controlling the Stormram 2: An MRI-compatible robotic system for breast biopsy," in *Proc. IEEE Int. Conf. Robot. Autom.*, 2017, pp. 1746–1753, doi: 10.1109/ICRA.2017.7989206.

[171] M. E. M. K. Abdelaziz et al., "Toward a versatile robotic platform for fluoroscopy and MRI-guided endovascular interventions: A pre-clinical study," in *Proc. IEEE/RSJ Int. Conf. Intell. Robots Syst. (IROS)*, 2019, pp. 5411–5418, doi: 10.1109/IROS40897.2019.8968237.

[172] N. Yu, C. Hollnagel, A. Blickenstorfer, S. S. Kollias, and R. Riener, "Comparison of MRI-compatible mechatronic systems with hydrodynamic and pneumatic actuation," *IEEE/ASME Trans. Mechatronics*, vol. 13, no. 3, pp. 268–277, Jun. 2008, doi: 10.1109/TMECH.2008.924041.

[173] H. Su, G. A. Cole, and G. S. Fischer, "High-field MRI-compatible needle placement robots for prostate interventions: Pneumatic and piezoelectric approaches," in *Advances in Robotics and Virtual Reality*, T. Gulrez and A. E. Hassanien, Eds., Berlin, Germany: Springer Berlin Heidelberg, 2012, pp. 3–32.

[174] D. Morrison et al., "Cartman: The low-cost cartesian manipulator that won the amazon robotics challenge," in *Proc. IEEE Int. Conf. Robot. Autom.*, Sep. 2018, pp. 7757–7764, doi: 10.1109/ICRA.2018.8463191.

[175] Y. Wang, K. W. Kwok, K. Cleary, R. H. Taylor, and I. Iordachita, "Flexible needle bending model for spinal injection procedures," *IEEE Robot. Autom. Lett.*, vol. 8, no. 3, pp. 1343–1350, Mar. 2023, doi: 10.1109/LRA.2023.3239310.

[176] G. Li et al., "Robotic system for MRI-guided stereotactic neurosurgery," *IEEE Trans. Biomed. Eng.*, vol. 62, no. 4, pp. 1077–1088, Apr. 2015, doi: 10.1109/TBME.2014.2367233.

[177] S. Uğurlu, E. Baysoy, and M. Kocakulak, "Magnetic resonance imaging compatible biomaterials for realization of interventional operations," *Natural Appl. Sci. J.*, vol. 3, pp. 94–101, Jan. 2021.

[178] D. R. Marker et al., "1.5 T augmented reality navigated interventional MRI: Paravertebral sympathetic plexus injections," *Diagnostic Interventional Radiol.*, vol. 23, no. 3, pp. 227–232, 2017, doi: 10.5152/dir.2017.16323.

[179] J. Fu et al., "Augmented reality and human–Robot collaboration framework for percutaneous nephrolithotomy: System design, implementation, and performance metrics," *IEEE Robot. Autom. Mag.*, early access, 2024, doi: 10.1109/MRA.2024.3358721.